Determination of Density and Viscosity of Fluids and Fluid Mixtures using Frequency Response of Microcantilevers

by

Gamze Eriş

A Thesis Submitted to the

Graduate School of Sciences and Engineering

in Partial Fulfillment of the Requirements for

the Degree of

Master of Science

in

Chemical and Biological Engineering

Koc University

July 2015

Koc University

Graduate School of Sciences and Engineering

This is to certify that I have examined this copy of a master's thesis by

Gamze Eriş

and have found that it is complete and satisfactory in all respects,
and that any and all revisions required by the final
examining committee have been made.

Committee Members:

_____

Can Erkey, Ph. D. (Advisor)

_____

Alexandr Jonáš, Ph. D.

_____

Erdem Alaca, Ph. D.

Date: _____

to my family…

ABSTRACT

In this study, we investigate the resonant frequency and Q-factor of ferromagnetic nickel microcantilever immersed in Ar, N_2, CO_2 and CO_2-N_2 binary mixtures at 308.15 K and pressures up to 24 MPa. Measurements were performed using an experimental setup that includes a temperature controlled high-pressure vessel which can operate within a temperature range of 273 – 423 K and a pressure range of 1 – 30 MPa. A microchip containing microcantilevers and an electromagnet for microcantilever actuation were placed inside the vessel. The procedure followed for the determination of microcantilever frequency response then involved driving of microcantilevers with AC magnetic field at varying frequencies and detecting of the corresponding laser deflections from the driven cantilevers with a quadrant photodiode (QPD). At a constant temperature, resonant frequency and Q factor of microcantilever oscillations were found to decrease with increasing pressure as a result of increasing density and viscosity of the fluid. Experimental data was analyzed using Sader's model which describes oscillatory motion of immersed cantilevers incorporating the effects of density- and viscosity-dependent hydrodynamic forces. A very good agreement between the experimentally obtained cantilever resonant frequencies and quality factors and the predictions of Sader's model was observed. The low difference in experimental and theoretical values illustrates that our experimental approach is suitable for the density and viscosity measurement of gas and supercritical fluids and fluid mixtures at a wide range of pressures. Based on these results, we carried out simultaneous measurement of density and viscosity of nitrogen from the measured frequency responses of an oscillated microcantilever immersed in N_2. To this end, using argon as a reference fluid of known density and viscosity, cantilever calibration parameters were obtained from nonlinear regression of cantilever resonant frequencies and quality factors recorded in argon. Subsequently, these calibration parameters were used in the

model equations to determine the density and viscosity of nitrogen at the given experimental pressure and temperature. In the studied pressure range, the root-mean-square deviations of the measured density and viscosity of nitrogen from the reference values obtained from NIST database were 2.5% and 5.2%, respectively. Finally, we studied thermophysical properties of more complex fluid systems represented by fluid mixtures. In order to investigate the density and viscosity of fluid mixtures, CO_2-N_2 binary mixture was chosen as a model fluid. The average relative deviation range for different compositions of CO_2-N_2 binary mixture was found to be 0.96 % -13.27 % for density and 2.42 %- 15 % for viscosity when N_2 was used as reference fluid.

ÖZET

Bu çalışma yüksek basınçta gazlarda ve süperkritik akışkanlarda mikro mekanik çubuklar kullanılarak ağdalık ve yoğunluk ölçümü yapılan ilk çalışmadır. Bu çalışmada, mikro-çubukların argon, nitrojen, karbondioksit ve karbondioksit-nitrojen karışımları içindeki çınlanım sıklığı (f_0) ve nitelik katsayıları (Q) 308.15 K sıcaklıkta 24 MPa basınca kadar araştırıldı. Ölçümler 273-423K sıcaklığa ve 300 atm basınca dayanıklı yüksek basınçlı kapta ölçümler yapılmıştır. Mikromekanik çubukların bulunduğu mikro çip ve elektromagnetyüksek basınçlı kabın içerisine yerleştirilmiştir. Ölçümler, mikroçubukların alternative akımlı manyetik alanda hareket ettirilmesi sonucu quadrant fotodiyot ile laserin sapması prosedürüyle elde edilmiştir. Sabit sıcaklıkta, çınlanım sıklığı ve nitelik katsayılarının basınç artışıyla azaldığı görülmüştür. Deneysel sonuçlar salınan mikroçubukların hidrodinamik kuvvetleri hesaba katarak davranışını tanımalayan Sader'ın modeli ile karşılaştırılmıştır. Deneysel olarak elde edilen çınlanım sıklığı ve nitelik katsayılarını değerleri Sader'ın modeli kullanlarak elde edilen değerlere yakın bulunmuştur. Bu değerlerin yakın olması deneysel olarak izlenen yolun, gaz ve süperkritik akışkan ve akışkan karışımlarında yoğunluk ve ağdalık ölçümleri için uygun olduğunu gösterir. Çınlanım sıklığı ve nitelik katsayısı kullanılarak nitrojenin ağdalık ve yoğunluk ölçümleri bildirilmiştir. Öncelikle yoğunluk ve ağdalık değeri bilinen argon ile referans ölçüm alınarak kalibrasyon parametreleri saptanmıştır. Daha sonra, bu kalibrasyon parametreleri model denklemlerinde kullanılarak istenen sıcaklık ve basınçta nitrojenin ağdalık ve yoğunluk değeri bulunmuştur. Çalışılan başınç aralığında, yoğunluk ve ağdalık değerleri NIST veritabanındaki değerlerle karşılaştırılmış, kök ortalama kare sapması çınlanım sıklığı ve nitelik katsayısı için 2.5% and 5.2% olarak bulunmuştur.Akışkan karışımlarını incelemek adına CO_2-N_2 karışımı model karışım olarak seçilmiştir. Bu karşımda ağdalık ve yoğunluk ölçümü nitrojen referans akışkan kullanılarak yapılmış, göreceli sapma değer aralığı yoğunluk değerleri için 0.96 % -13.27 % ve ağdalık değerleri için 2.42 %- 15 % bulunmuştur.

ACKNOWLEDGEMENTS

First and foremost, I would like to thank my advisor Professor Can Erkey for his guidance, encouragement, supervision and support since I came to Koç University. He inspired me to follow an academic career with his experience, great knowledge, kindness and friendly attitude. I am honored to be a member of his research group for six years including my undergraduate. I would like thank Prof. B. Erdem Alaca, Asst. Prof. Alexandr Jonáš and Prof. Alper Kiraz for their generous guidance in the fields of mechanics and optics and for encouraging me to learn and ask more questions.

I also would like to thank my colleagues Deniz Şanlı, Selmi Bozbağ, Zeynep Ülker Demir, Yaprak Özbakır and Göktuğ Gönel for their help, support, and friendship in the research laboratory. I would thank specially to Deniz Şanlı who helped, guided and taught many things in the laboratory.

I would also like to thank to all my friends in Koç University, to name some, Perfecto9, Benay Uzer, Çiğdem Altıntaş and Didar Aşık and my house mates who made all these years an enjoyable period of time with their support and friendship.

Above all, I would like to thank my family for their endless love and support throughout my life. I am grateful for their friendship, enthusiasm, encouragement and understanding. I would like to thank specially to my love, Aytaç Uzun for his love and friendship. I thank god that I am surrounded with such a beautiful family full of love.

TABLE OF CONTENTS

LIST OF TABLES

LIST OF FIGURES

NOMENCLATURE

f_R	resonant frequency
Q	quality factor
f_{fluid}	dissipation free resonant frequency
ω_{fluid}	angular dissipation free resonant frequency
g	resonance half-line width
A_{max}	maximum amplitude
AFM	Atomic Force Microscopy
ω_{vac}	vacuum resonant frequency
w	cantilever width
ρ_c	cantilever density
t	cantilever thickness
ρ	density of the fluid
μ	viscosity of the fluid
QPD	Quadrant photodiode detector
A_0	zero-frequency amplitude
T_c	critical temperature
$\omega_{fluid,exp}$	experimental values of the cantilever angular resonant frequency
Q_{exp}	experimental values of the cantilever quality factor
$\omega_{fluid,calc}$	calculated angular resonant frequency
Q_{calc}	calculated quality factor
α	coefficient of thermal expansion
β	coefficient of thermal dependence of the elastic modulus

Chapter 1

INTRODUCTION

The knowledge/information about the thermophyiscal properties of the mixture under the conditions of the particular process will allow identification of possibly encountered problems, specification of safe concentration limits for the involved impurities, and definition of the requirements for purification and designing efficient, safe and economic processes. In this study, CO_2 - N_2 Binary mixture was chosen as a model fluid to predict the mixtures properties. CO_2 - N_2 Binary mixture has many applications in fossil fuel industries and supercritical fluid technologies. In these applications, CO_2 - N_2 binary mixture is used at high pressures, and limited data is available in the literature to investigate the properties at high pressures .For example, the density and viscosity information/properties are required for N_2- CO_2 separation in CO_2 capture and storage (CCS) systems. The purpose of CO_2 capture is to produce a concentrated stream of CO_2 at high pressure ready for storage. For that purpose, impurities should be removed in either in the pre-combustion or in the post-combustion processes such as nitrogen(N_2) and argon(Ar)[1].

There are many different viscometers and densimeters developed to measure density and viscosity at high pressures. Some of the common types of viscometers are capillary tube viscometer, falling body viscometer, rolling ball viscometer, rotational viscometer,oscillating body viscometer and vibrating wire viscometers. Some of common type of densimeters are buoyancy type densitometer, vibrating element densitometers and

vibration tube densitometers. Even though there are many experimental techniques available to measure separately the density and viscosity of fluids with a high precision over a wide range of fluid pressures[2, 3], there is a growing interest to develop new techniques for simultaneous measurement of the density and viscosity. This is partly being driven by the necessity to know the fluid density in order to extract the viscosity from the raw experimental data and working equations employed in nearly all viscometers. Moreover, almost all of the thermodynamic correlations developed for the prediction of viscosity of a particular fluid contain density. Moreover, viscometers/densitometers based on vibrating or rotating macroscopic probes (wires, cylinders, or balls) are quite complex to construct and operate and require large sample volumes. Therefore, microcantilever-based sensors are an attractive alternative for characterization of low volumes of target fluids with inherent high sensitivity, fast response, simple and compact architecture.

To extract density and viscosity, microcantilevers are oscillated with external driving and change in the frequency response of the cantilevers is related to density and viscosity. In this approach, the cantilever in resonance is exposed to the hydrodynamic force exerted by the surrounding gas molecules. This mechanical interaction with the surrounding gas affects the resonant behavior of the cantilever through the added mass effect due to the inertia of the gas and energy dissipation effect due to the viscous drag. As both effects are related to the density and viscosity of the specific gas, this approach enables one to relate both the density and the viscosity of pure fluids or mixtures to the frequency response of the cantilever [4].

Frequency response of an oscillating cantilever can be characterized by its resonant frequency, ω_R, and the quality factor of the oscillations, Q-factor. ω_R is defined as the angular frequency at which the maximum amplitude of driven cantilever oscillations is observed. Q-factor is determined by the spectral bandwidth of the cantilever frequency response. It is formulated as $Q=f_R/2g$, in which the frequencies f_R+g and f_R-g above and below

f_R at which the amplitude is equal to $A_{max} / \sqrt{2}$, where A_{max} is the maximum amplitude of oscillation achieved at f_R, as shown in Figure 1.1. Q-factor quantifies energy dissipation during oscillation.

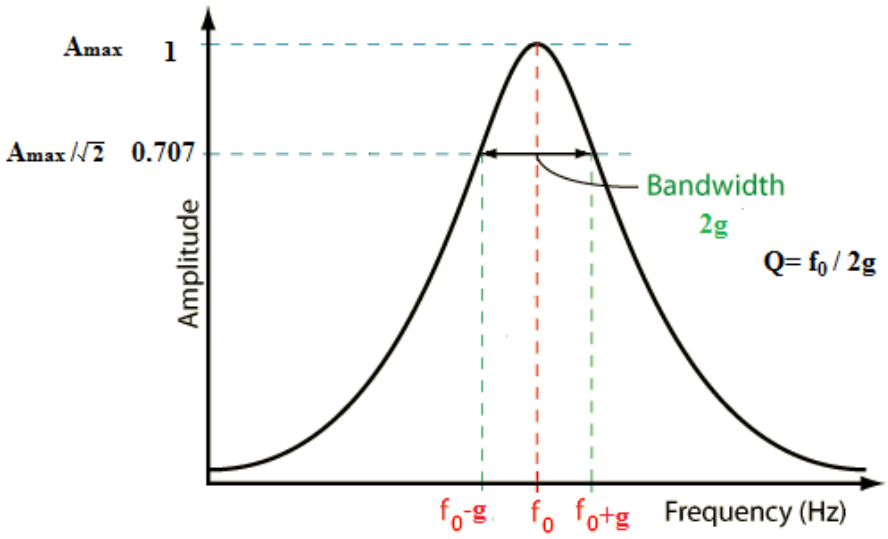

Figure 1.1 : Cantilever Frequency Response

This thesis is composed of five chapters.

Chapter 2 reviews operating principles of densimeters and viscometers and studies on density and viscosity measurement, and composition detection using microcantilevers. Chapter 3 presents the experimental setup and measurement technique for recording frequency responses of microcantilevers immersed in the studied fluid. In Chapter 4, resonant frequency and Q-factor measurements of Ar,CO_2 ,N_2, CO_2 - N_2 mixture are presented and compared with the theoretical model. Using this model, density and viscosity of target fluid is determined using a reference fluid. Chapter 5 summarizes the results, and presents the suggestions for future work.

Chapter 2

LITERATURE REVIEW

Characterization of fluid density and viscosity

There is a growing interest in accurate density and viscosity measurements at high pressures due to the increase in the high pressure processes in various industries. Moreover, knowledge of density and viscosity of pure fluids and fluid mixtures at high pressures is important not only for the development of supercritical fluid-based technological processes but also for understanding the nature of intermolecular interactions at supercritical conditions.

In this chapter, some of the common types of viscometers and densimeters operating at high pressures are introduced and their main characteristics and limitations are summarized.Moreover, microcantilevers for simultaneous density and viscosity measurement is introduced and theory of simple damped harmonic oscillator is explained.

2.1 Viscometers and densimeters for measurements at high pressure

Capillary Viscometer

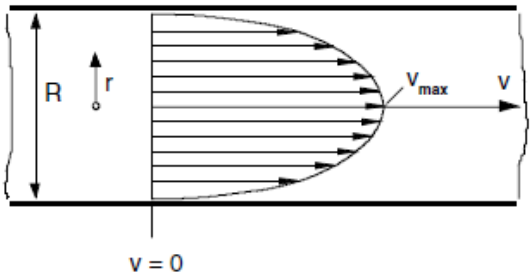

Figure 2.1 Velocity profile of the laminar flow [5]

A capillary viscometer consists of a cylindrical tube whose length *L* is much larger compared to the very small radius *R*. This minimizes the end (entrance and exit) effects on the flow. The principle of the operation is based on p measuring flow rate through the capillary and the pressure difference between the both end of the capillary tube of the liquid. The flow in the tube should be laminar. (See Figure 2.1) Liquid is considered as incompressible.

Under these conditions, for Newtonian fluids, the principle of viscometers is based on Hagen-Poiseuille Law [5-7].

$$\gamma = \frac{\mu}{\rho} = \frac{\pi R^4 g h_m}{8LV} t = K t \quad (2.1)$$

where γ is the kinematic viscosity, h_m is the mean pressure height, V is volume and t is flow time

As it is seen in Eq. 2.1, kinematic viscosity depends on the flow time and constants and geometric parameters. These constants and geometric parameters are specific to the viscometer; thus these parameters are called viscometer constant, K. Since the measurements provide a kinematic viscosity, density of the fluid should be known accurately to obtain dynamic viscosity. The main advantage of using the capillary viscometers is to obtain measurements easily and directly. However it is difficult to detect small pressure drop values precisely while maintaining a laminar flow. Many types of

designs were developed to maintain the laminar flow. One type of capillary viscometer is given in Figure 2.2.

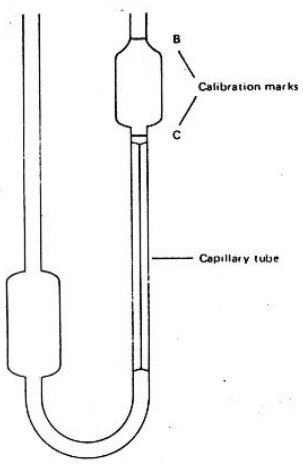

Figure 2.2. Ostwald capillary viscometer[8]

Falling body viscometer

Falling body viscometer is based on a body of known shape, size, and density which is allowed to fall in the studied fluid due to gravity (see Figure 2.3). Once the body is allowed to descend in the fluid, the surrounding fluid provides resistance which is directly proportional to the instantaneous velocity of the body and the fluid viscosity. Eventually, the forces of gravity and fluid viscous friction balance each other and the body moves with a constant terminal velocity. Recording the time needed by the body to travel the distance between given start and end points then enables to find the average velocity of the body during the fall. With known values of density and size of the body, density of the liquid, and average velocity of the body, viscosity can be calculated using Stoke's Law. The shape of the body is typically sphere, cylinder, ball or needle [6, 7, 9].

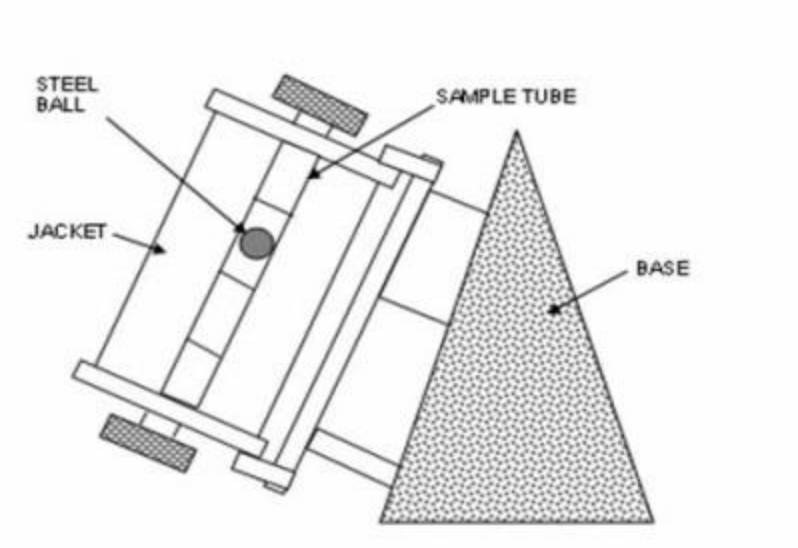

Figure 2.3. Schematic of Falling Ball Viscometer [10]

Measurements at high pressures were done in high pressure vessels. In order to ensure that the body falls freely and vertically, a vessel and sample of sizable volume is required.

Rolling Ball Viscometers

In rolling ball viscometers, a spherical object is allowed to descend with a slow rate in an inclined trajectory inside a tube filled with the studied fluid. It is different from falling body viscometers in terms of the rate of fall along the path and the fact that the object is in contact with a solid wall while moving through the fluid. The spherical object originally at rest eventually reaches a constant velocity as it descends. At this steady state, gravitational force is equal to the sum of buoyant and viscous forces. At high pressures, the movement of the body is monitored through sapphire or diamond windows connected to the vessel. The body may also slip rather than roll during the measurement which will cause errors in the results [6, 7, 9]

Rotational Viscometers

Operation of rotational viscometers is based on the fact that torque required to turn an object in a fluid is a function of fluid viscosity. The viscometer gives the required force necessary to turn the rotor immersed in the studied fluid at a constant and known speed. Alternatively, the time needed for the rotor to decelerate from a constant initial angular velocity to zero when the driving is turned off can be measured. There are different designs of rotational viscometers. In cup and bob viscometers, the studied fluid is placed between two concentric cylinders and either outer cylinder is fixed and inner cylinder is rotating (Searle system) or outer cylinder is rotating and inner cylinder is fixed (Couette System). There are also cone and plate viscometers which make use of the shear between a flat plate and a cone. From shear stress versus shear rate graph viscosity can be obtained. Rotational viscometers are very suitable for measuring the viscosity of Non-Newtonian fluids[6, 11].

Oscillating Body Viscometers

In oscillating body viscometers, a symmetrical body is suspended within a vessel containing the studied fluid. When the body is oscillated in the fluid, gradual damping of the motion is observed. Damping occurs due to the viscous coupling of the liquid to the vessel, viscous coupling between the layers in the fluid and the frictional losses coming from the system. The amplitude and time periods of the oscillation is recorded. With the help of reliable theoretical equations, viscosity can be related to the period and decrement of the amplitude. The shapes of the oscillating bodies commonly used in the studies are sphere, discs and cylinders. Oscillating body viscometers are constructed easily and can measure viscosity of both gases and liquids. However developing accurate mathematical expressions is difficult and requires corrections terms[12].

Vibrating Wire Viscometers

In vibrating wire viscometers, wire that is immersed in the fluid is electromagnetically actuated and the damping of the resonator is related to the viscosity. There are different ways of measuring damping in the system. One way is to measure the decay time/rate of the oscillation after excitation is turned off. Another is to measure the power input to vibrate the resonator at constant amplitude. Different from other types of viscometers discussed above, these instruments are mechanically simpler and they don't require bulk volume of fluid. Measurement at high pressures and temperatures can be done for fluids and fluid mixtures[6].

Buoyancy type densitometer

In buoyancy type densitometers, a mass (sinker) with a known volume and mass is suspended by a wire and immersed in a fluid. The force supporting the sinker is measured with a balance. Fluid density is then calculated from the known mass and volume of the sinker and the measured force supporting the weight of the sinker. One advantage of using this type of densitometer is the use of magnetic suspension system where the all system is in the fluid eliminating surface effects[13].

Vibrating Element Densitometers

Vibrating element densitometers operate based on the fact that the natural resonant frequency of a body immersed in the studied fluid depends not only on the mechanical and geometrical properties of the body but also on the characteristics of the fluid surrounding

the body. The vibrating element can be approximated by a mass-spring system and the density-dependent resonant frequency can be written as follows[13].

$$f = \sqrt{\frac{K}{m+k\rho}} \tag{2.2}$$

where *K* is the system stiffness,*m* is the transducer mass, *k* is the system constant, and ρ is the fluid density.

Vibrating Tube Densitometer

In vibrating tube densitometers, a thin tube is oscillated transversally at its fundamental resonant frequency by an electromagnetic actuator (see Figure 2.4). During the motion, the liquid goes into the tube, thus changing its effective mass. Subsequently, the density of the fluid trapped between the oscillation nodes can be measured from shifts in the tube resonant frequency [13].

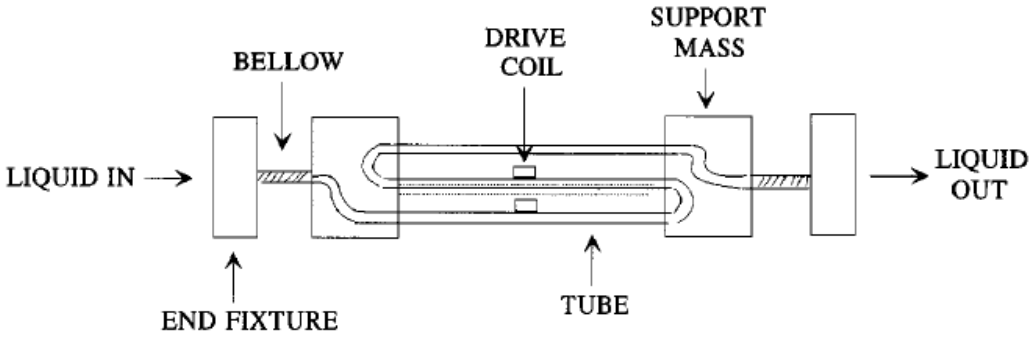

Figure 2.4. A schematic of vibrating tube densitometer [13]

2.1.2 Densimeters/Viscometers for Simultaneous Measurements

Even though there are many experimental techniques available to measure separately the density and viscosity of fluids with a high precision over a wide range of fluid pressures[2, 3], there is a growing interest to develop new techniques for simultaneous measurement of the density and viscosity. This is partly being driven by the necessity to know the fluid density in order to extract the viscosity from the raw experimental data and working equations employed in nearly all viscometers. Moreover, almost all of the thermodynamic correlations developed for the prediction of viscosity of a particular fluid contain density. Parallel measurements of fluid density and viscosity were carried out using, for example, a rotating-body viscometer[14] or a vibrating-wire viscometer [15] combined with an independent vibrating-tube densitometer. However, the use of two separate instruments can introduce error into the measured values caused by the difficulty to maintain exactly identical experimental conditions (i.e. the fluid pressure and temperature) in both instruments. In addition, independent measurements increase required measurement time and volume of the fluid. To address these issues, Padua and co-workers carried out simultaneous viscosity and density measurements with a vibrating-wire viscometer modified by attaching a suspended buoyant body (a sinker) directly to the vibrating wire [16, 17]. The presence of the sinker changed the wire tension in a density-dependent way, resulting in measurable shifts of the wire resonant frequency. A vibrating-wire viscometer in combination with a single-sinker densitometer was adopted by Seibt et al. to measure the viscosity and density of helium and nitrogen over a wide range of temperatures and pressures [18]. Krall and Sengers employed a disk suspended from a torsion wire oscillating in the studied fluid to determine the fluid density and viscosity from the measured period and amplitude damping factor of the disk oscillations [19]. However, coupling between the disk oscillation period and damping factor in the working equations

describing the system reduced the precision of the measurement for certain viscosity-to-density ratios. Evers et al. used magnetic coupling to suspend a cylindrical sinker in a fluid and transfer the buoyant forces acting on it to an external microbalance to determine the fluid density [20]. At the same time, fluid viscosity was extracted from the rate of decay of the rotational velocity of the sinker. In general, combined viscometers/densitometers based on vibrating or rotating macroscopic probes (wires, cylinders, or balls) are quite complex to construct and operate and require large sample volumes.

2.2 Microcantilevers for Density and Viscosity Measurement

Oscillated microcantilevers have shown a great potential for applications as devices for the simultaneous measurement of fluid density and viscosity, providing a high sensitivity, fast response, simple and compact structure, and low sample requirements down to microliter and even nanoliter range [21, 22].

For applications where gas sensing is of interest, two approaches are frequently employed. The first approach involves coating of the cantilever surface with a sensitive layer such as a polymeric thin film or an inorganic porous material including nanotubes with affinity to the gaseous species of interest. The sorption or binding of the gas molecules on the sensitive surface leads to a change in the effective mass of the cantilever and thus its resonant frequency [23]. This approach is usually used to detect trace amounts of gases or volatile compounds in mixtures. For example, Baselt et al investigated hydrogen sensing using Pd-Ni coated cantilevers and they detected the presence of hydrogen in the concentration range of 0.1% and 100% [24]. In this approach the measurements are usually performed at room temperature and atmospheric pressure, where the interaction between the sensing element and the target gas can be low. Moreover, it can be hard to detect highly inert substances such as nitrogen using functionalized surfaces.

The second approach involves pure substances or mixtures, whose physical properties are to be determined. In this approach, the cantilever in resonance is exposed to the hydrodynamic force exerted by the surrounding gas molecules. The hydrodynamic force consists of two components: pressure (normal to the vibrating surface) and viscous force (tangential to the vibrating surface). This mechanical interaction with the surrounding gas affects the resonant behavior of the cantilever through the added mass effect due to the inertia of the gas and energy dissipation effect due to the viscous drag. As both effects are related to the density and viscosity of the specific gas, this approach enables one to relate both the density and the viscosity of pure fluids or mixtures to the frequency response of the cantilever. This approach also facilitates the determination of concentration of an ingredient in a binary gas mixture [4].

The frequency response of cantilevers suspended in viscous medium has been studied experimentally and theoretically, and density and viscosity has been related with the resonant frequency and quality factor using various models of immersed cantilever motion. The most rigorous approach to the problem proposed by Sader is based on the solution of the equation of motion of a clamped elastic beam subject to hydrodynamic forces of the surrounding fluid [25]. The complete solution developed by Sader was subsequently simplified by Maali et al.[26] who derived an analytical approximation to the transcendental hydrodynamic function of Sader, resulting in Eq. (2.3) and (2.4) for the dissipation-free cantilever angular resonant frequency ω_{fluid} and quality factor Q:

$$\omega_{fluid} = \omega_{vac}\left[1 + \frac{\pi\rho w}{4\rho_c t} * \left(1.0553 + 3.7997\sqrt{\frac{2\mu}{\rho\omega_{fluid}w^2}}\right)\right]^{-1/2} \quad (2.3)$$

$$Q = \frac{\frac{4\rho_c t}{\pi\rho w} + \left(1.0553 + 3.7997\sqrt{\frac{2\mu}{\rho\omega_{fluid}w^2}}\right)}{3.8018\sqrt{\frac{2\mu}{\rho\omega_{fluid}w^2}} + 2.7364\frac{2\mu}{\rho\omega_{fluid}w^2}} \quad (2.4)$$

Here, ρ is the fluid density, μ is the fluid viscosity, w is the width of the cantilever, ρ_c is the cantilever density, t is the cantilever thickness, ω_{vac} is the vacuum angular resonant frequency, and the dissipation-free cantilever angular resonant frequency ω_{fluid} is related to the actual angular resonant frequency of the damped cantilever in the fluid ω_R (i.e. the angular frequency of the maximal measured amplitude of the cantilever oscillations) by

$$\omega_{fluid} = \omega_R/\sqrt{1 - 1/2Q^2}. \quad (2.5)$$

For sufficiently large quality factors (small dissipation), oscillating cantilever can be approximated as a simple damped harmonic oscillator and the resonant frequency ω_{fluid} and Q-factor can be obtained from fitting the measured frequency response of the cantilever to the harmonic oscillator formula 2.28 which is provided in the next section.

2.2.1. Frequency response of a damped Harmonic Oscillator

Oscillatory motion is the periodically repeating motion. The motion is described by its amplitude, frequency and period (see Figure 2.5). Amplitude (A) is the maximum distance of vibration or oscillation from the equilibrium point. Period (T) is the time required between consecutive occurrences of the same state (1 cycle) in an oscillatory motion. Frequency (f) is the number of cycles per unit time.

$$f = \frac{1}{T} \quad (2.6)$$

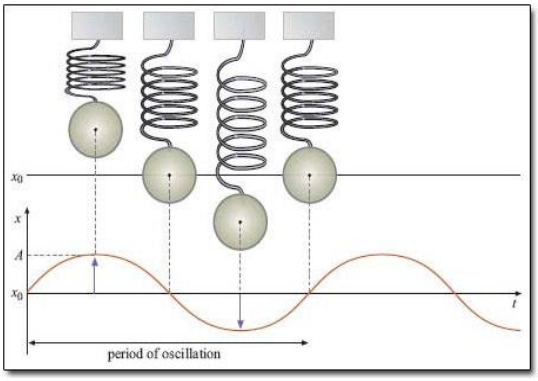

Figure 2.5.Oscillatory Motion of Simple Harmonic Oscillator

The simplest harmonic oscillator can be formed by attaching mass m to a spring (see Figure 2.5). When the mass is displaced from its equilibrium position by a distance x, it experiences a restoring force $F_{restoring}$ from the spring which is directly proportional to the displacement. This relationship $F_{restoring} = -kx$ is know as Hooke's Law with the proportionality constant k called the stiffness or force constant of the spring. The direction of the restoring force is given in Figure 2.6

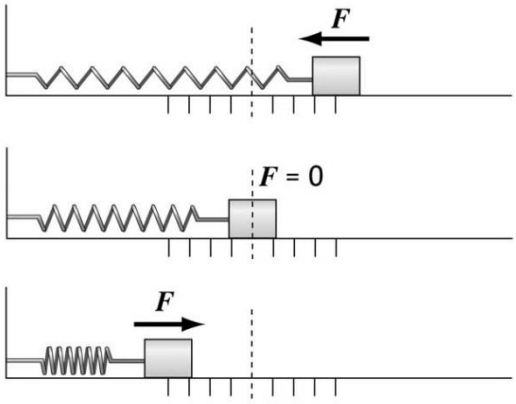

Figure 2.6. Restoring force in Mass-Spring system

Simple Harmonic Oscillator (SHO)

For SHO, the net force acting on the oscillating mass is equal to the restoring force of the spring described by Hooke's Law[27, 28]:

$$F_{net} = F_{restoring} = -kx \tag{2.7}$$

From Newton's second law,

$$F_{net} = ma = m\,\frac{d^2x}{dt^2} \tag{2.8}$$

which can be rewritten as

$$-k\,x = m\frac{d^2x}{dt^2} \qquad \text{or} \qquad \frac{d^2x}{dt^2} + \frac{k}{m}x = 0 \tag{2.9}$$

Introducing undamped natural frequency $\omega_o = \sqrt{k/m}$, we finally obtain the equation of motion of SHO in the form

$$\frac{d^2x}{dt^2} + \omega_0^2 x = 0 \quad (2.10)$$

The solution to Eq. 2.10 is found as

$$x(t) = A\sin(\omega_o t - \varsigma) \quad (2.11)$$

where A is the amplitude and ς is the phase of oscillations which occur with frequency ω_0.

Simple Damped Harmonic Oscillator (SDHO)

In addition to the restoring force $F_{restoring}$, SDHO experiences friction force $F_{friction}$ which always opposes the motion of the oscillating mass[27, 28]:

$$F_{friction} = -c\,v \quad (2.12)$$

where c is the viscous damping coefficient and $v = \frac{dx}{dt}$ is the velocity of the moving mass. Thus, the net force acting on the moving mass is $F_{net} = F_{restoring} + F_{friction}$ and the equation of motion reads as

$$-k\,x - c\frac{dx}{dt} = m\frac{d^2x}{dt^2} \quad (2.13)$$

which can be rearranged as

$$\frac{d^2x}{dt^2} + \frac{c}{m}\frac{dx}{dt} + \frac{k}{m}x = 0 \quad (2.14)$$

Introducing damping ratio ζ as

$$\zeta = \frac{c}{c_c} \quad (2.15)$$

where the critical viscous damping coefficient $c_c = 2\sqrt{mk} = 2m\omega_o$

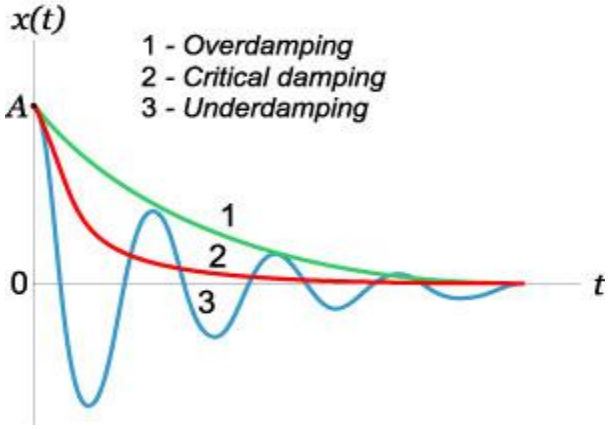

Figure 2.7. Damping in the oscillatory motion

we finally arrive at the equation of motion for SDHO in the form

$$\frac{d^2x}{dt^2} + 2\,\zeta\,\omega_o\,\frac{dx}{dt} + {\omega_0}^2 x = 0 \qquad (2.16)$$

The solution to Eq.2.16 is given by

$$x(t) = e^{-\beta t}(A_1 e^{\sqrt{\beta^2-{\omega_0}^2}t} + A_2 e^{-\sqrt{\beta^2-{\omega_0}^2}t}) \qquad (2.17)$$

where $\beta = \zeta\,\omega_o$.

Figure 2.7 illustrates the dependence of oscillator displacement on time for various values of ζ. In particular, overdamped scenario corresponds to $\zeta > 1$, critical damping occurs for $\zeta = 1$, and underdamped case corresponds to $\zeta < 1$. According to Eq. 2.17, damped oscillations occur for $\zeta < 1$ with a frequency $\omega_d = \sqrt{\omega_0^2 - \beta^2}$ which is lower than the undamped natural resonant frequency ω_0 due to the effects of viscous friction which slows down the oscillatory motion.

Driven Harmonic Osillators

When a sinusoidally-varying driving force with frequency ω and amplitude F_o

$$F_{drive} = F_o \cos \omega t \qquad (2.18)$$

is applied to the oscillator, the equation of motion can be written as follows:

$$\frac{d^2x}{dt^2} + 2\,\zeta\,\omega_o\,\frac{dx}{dt} + {\omega_0}^2 x = \frac{F_o}{m}\cos\omega t \tag{2.19}$$

The solution to inhomogeneous Eq. 2.19 can be found as a superposition of general solution $x_c(t)$ of the homogeneous equation 2.16 which represents transient effects and a particular solution $x_p(t)$ which represents the steady state effects[27, 28]:

$$x(t) = x_c(t) + x_p(t) \tag{2.20}$$

Complementary part of the solution $x_c(t)$ was found in the previous section and it is given in Eq. 2.17. For particular solution $x_p(t)$, solution in the following form is suggested:

$$x_p(t) = D\cos(\omega t - \varsigma) \tag{2.21}$$

where D is the amplitude of the displacement, ω is the driving frequency, and ς is the phase lag of the oscillator displacement with respect to the driving force.

Subsequently, Eq. 2.21 is substituted into Eq. 2.19 and rearranged:

$$\cos\omega t\{F_0/m - D[(\omega_0^2 - \omega^2)\cos\varsigma + 2\beta\omega\sin\varsigma]\} - \sin\omega t\{D(\omega_0^2 - \omega^2)\sin\varsigma - 2\beta D\omega\cos\varsigma\} = 0 \tag{2.22}$$

In order to fulfil equation 2.22 for an arbitrary value of $\cos\omega t$ and $\sin\omega t$, the expressions in the curly brackets must be equal to zero. Thus,

$$(\omega_0^2 - \omega^2)\sin\varsigma = 2\beta\omega\cos\varsigma \tag{2.23}$$

and, consequently,

$$\tan\varsigma = \frac{2\beta\omega}{{\omega_0}^2 - \omega^2} = \frac{\frac{2\beta\omega}{\sqrt{(\omega^2-\omega^2)^2+4\omega^2\beta^2}}}{\frac{{\omega_0}^2-\omega^2}{\sqrt{({\omega_0}^2-\omega^2)^2+4\omega^2\beta^2}}} \tag{2.24}$$

Similarly,

$$D = \frac{F_0/m}{(\omega_0^2-\omega^2)\cos\varsigma + 2\beta\omega\sin\varsigma} \tag{2.25}$$

When Eq. 2.24 is substituted into Eq. 2.25, we obtain the amplitude D(w) of driven oscillations as a function of driving frequency:

$$D(w) = \frac{F_0/m}{\sqrt{(\omega_0{}^2 - \omega^2)^2 + 4\omega^2\beta^2}} \tag{2.26}$$

The final solution for the displacement of a sinusoidally driven harmonic oscillator is

$$x(t) = x_c(t) + x_p(t) = e^{-\beta t}(A_1 e^{\sqrt{\beta^2 - \omega^2}t} + A_2 e^{-\sqrt{\beta^2 - \omega_0{}^2}t}) + \frac{F_0/m}{\sqrt{(\omega_0{}^2 - \omega^2)^2 + 4\omega^2\beta^2}} \cos(\omega t - \varsigma)$$

(2.27)

When the following substitutions are made:

$$\beta = \zeta\omega_o, \quad \zeta = \frac{1}{2Q}, \quad \beta^2 = \frac{\omega_0{}^2}{4Q^2}, \omega_o = \omega_{fluid} \quad , \; A_o = \frac{F_0/m}{\omega_0{}^2}$$

equation 2.26 for the amplitude of the frequency response of a driven harmonic oscillator can be transformed to the form

$$D(\omega) = \frac{A_o \omega_{fluid}{}^2}{\sqrt{(\omega^2 - \omega_{fluid}{}^2)^2 + \frac{\omega^2 \omega_{fluid}{}^2}{Q^2}}} \tag{2.28}$$

which is suitable for determination of the natural resonant frequency ω_{fluid} and Q-factor of oscillations of a driven micorcantilever immersed in a fluid from fitting of experimentally recorded data. In connection with Equations 2.3 and 2.4, characteristic parameters of the cantilever frequency response can then be used to determine the density and viscosity of the immersion fluid.

2.2.2 Theoretical and Experimental Studies on the Frequency Response of Cantilevers for Density and Viscosity Measurements at atmospheric pressure

Equation (2.3) was used by Toda et al. to investigate the frequency response of cantilevers immersed in carbon dioxide in the vicinity of the critical point [29]. Youssry et al.[30] incorporated Maali's approximations to Sader's model and derived analytical expressions for determination of density and viscosity from the measured resonant frequency and Q-factor. Youssry et al. did one time calibration with air to calculate the vacuum resonant frequency of their cantilever. Using analytical expressions, the density was calculated with 20% error for fluids with 100cp and with 50.9% for 500cp. The errors for viscosity were high, 10-50% up to 1.67-100Cp and 110% for 550 cp. The high errors may be due to the reason that the mass density, thickness and width were taken from the specification of the cantilever. Boskovic et al.[31] described a method for determining the density and viscosity of an unknown fluid using cantilever calibration with a reference fluid. The fit parameters - vacuum frequency and linear mass density - were calculated using reference measurement in air. The measurements were carried out at atmospheric pressure and 27 degree of Celsius temperature. The errors for density and viscosity for the gases and liquids were less than 14 %. McLoughlin et al. [32] used Boskovic's suggested method to determine the density and viscosity of a fluid mixture at ambient pressure and room temperature using reference measurements in air and two additional fluids with known properties. Shih et al. measured the density and viscosity of glycerol-water mixtures at different concentrations with a piezoelectric cantilevers of different lengths [33]. Wilson et al. [34] determined density and viscosity of 5%, 10%, 15%, and 20% glycerol solutions from frequency responses of piezoelectric millimeter sized cantilevers by changing the excitation voltages. Jacoby [35] presented an analytical model based on an approximation of the immersed cantilever as an oscillating sphere. The knowledge of

mechanical and electrical properties of the cantilever was not required; the model parameters were instead obtained from the calibration procedure. The cantilever was calibrated in a set of liquids with well-known properties. Benjamin et al.[36] used resonating nanomechanical cantilevers embedded in a microliter fluid cell as transducers for real-time viscosity and mass density measurements. Photothermal excitation of the cantilever was implemented, and the use of higher flexural modes of vibration was studied. The use of the proposed method to monitor polymerization reaction kinetics with microliter sample consumption was investigated.

Moreover, gas composition analyses for binary mixtures were also investigated using frequency response of oscillating microcantilevers. Loui et al. studied the distinction and detection of pure gases and binary mixtures by using two distinct physical mechanisms which are heat dissipation and resonant damping of cantilever in viscous regime [37]. Tetin et al. detected the concentration of CO_2/N_2 and He/N_2 binary gas mixtures using resonant frequency measurements by uncoated piezoresistive microcantilevers and analyzed the detection sensitivity by changing the geometry of the microcantilever[4]. Xu et al. [38] provided gas composition analysis from the viscous damping of cantilevers based on the equations that relate the resonant frequency shift to the molar mass of the unknown gas. However, in the proposed method, 20 % CO_2 concentration change in CO_2 -air mixture can be detected with only 0.05% (0.5%) resonant frequency shift which makes it difficult to get high sensitivity.

These studies on frequency responses of microcantilevers in viscous fluid were performed at atmospheric pressure and limited concentration ranges. However, studies for gas mixtures in high pressure region, and frequency response of supercritical fluid mixtures containing a wide range of composition are largely missing in the literature.

2.3 High-pressure measurements of fluid density and viscosity

In our recent study, we addressed the lack of experimental investigations of high-pressure density and viscosity of fluids with the use of microcantilever-based sensors and developed an experimental set-up and protocols for measuring frequency response of cantilevers immersed in high-pressure fluids [5]. Frequency response of microcantilevers immersed in gas, liquid and supercritical phases of CO_2 in the temperature range 298 – 323 K and pressures up to 27 MPa were successfully measured and compared to the predictions derived from Maali's approximation to Sader's model of immersed cantilever motion. We observed a very good agreement between the experimentally obtained resonant frequencies and quality factors and the predictions of Sader's model, indicating that upon proper calibration, it might be possible to measure simultaneously the fluid density and viscosity at high pressures.

In this thesis, we report on the measurement and analysis of microcantilever frequency responses in nitrogen (N_2) and argon (Ar) in gas and suercritical phases at the temperature of 308.15 K and pressures up to 24 MPa. Using A as a reference fluid of precisely known density and viscosity, we calibrate the chaacteristic material and geometric parameters of the cantilever sensor. Next, we use these calibration parameters to determine the viscosity and density of N_2 at varying pressure from the frequency responses of the cantilever immersed in this fluid. We also invstigate the frequency response of microcantilevers in gas and supercritical mixtures of CO_2 and N_2 at high pressures. Resonant frequency and Q-factor values for different comositions of CO_2 – N_2 binary mixture are successfully obtained. Using N_2 as a reference fluid, we calibate the characteristic material and geometric parameters of the catilever sensor. The density and viscosity of CO_2 – N_2 binary mixture is calculated using the frequency response of microcantilevers and calibration parameters. Morever, the proposed method predicts the composition of the unknown concentration of binary mixtures using microcantilevers.

Chapter 3
Experimental Setup and Procedure

3.1 Experimental Setup

Frequency response measurements were performed with the home-made experimental setup shown in Figure 3.1

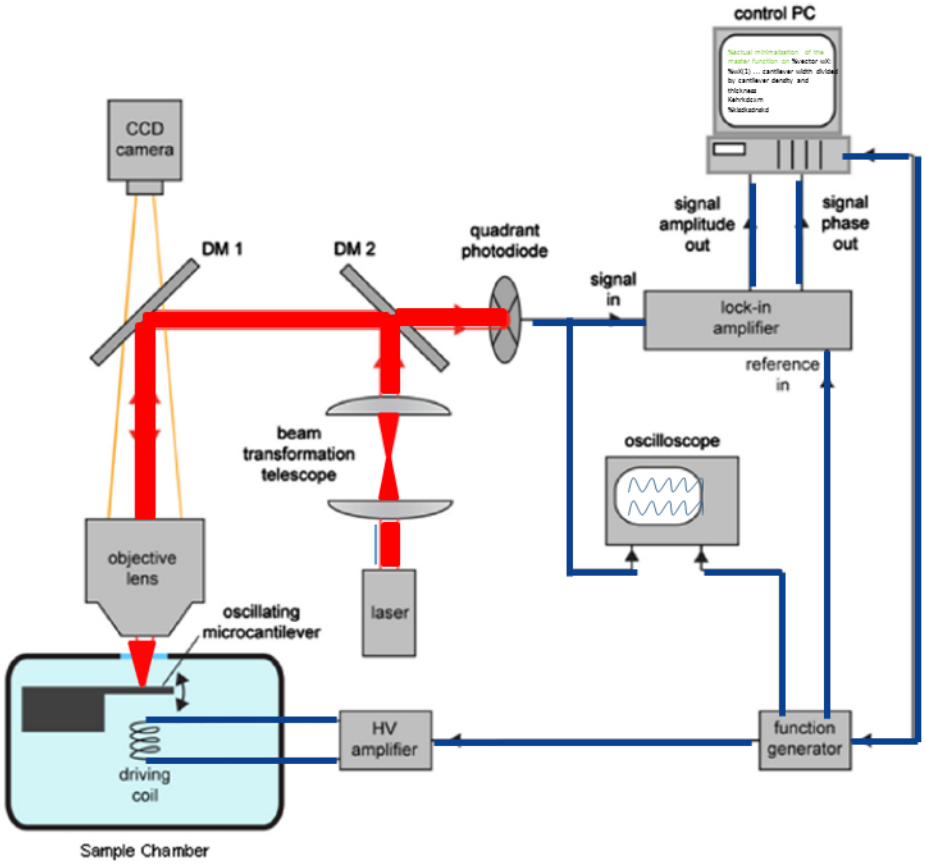

Figure 3.1 Schematic Presentation of the Experimental Setup

The electronic and optical parts of the experimental set up are shown in Figure 3.4 and Figure 3.5.

Figure 3.2: The experimental setup. Electronic Equipments (a) Agilent 33220A Arbitrary Waveform Function generator (b) Display (c)Tektronix TDS 1012 TDS 2000C Oscilloscope (d) Stanford Research Systems SR530 Dual Phase Lock in Amplifier (e) National Instruments USB 6008 Data Acquisition apparatus (f) Voltage Detection system connected to QPD (Quadrant Photodiode Detector) (g) Falco System High Voltage Amplifier WMA-300

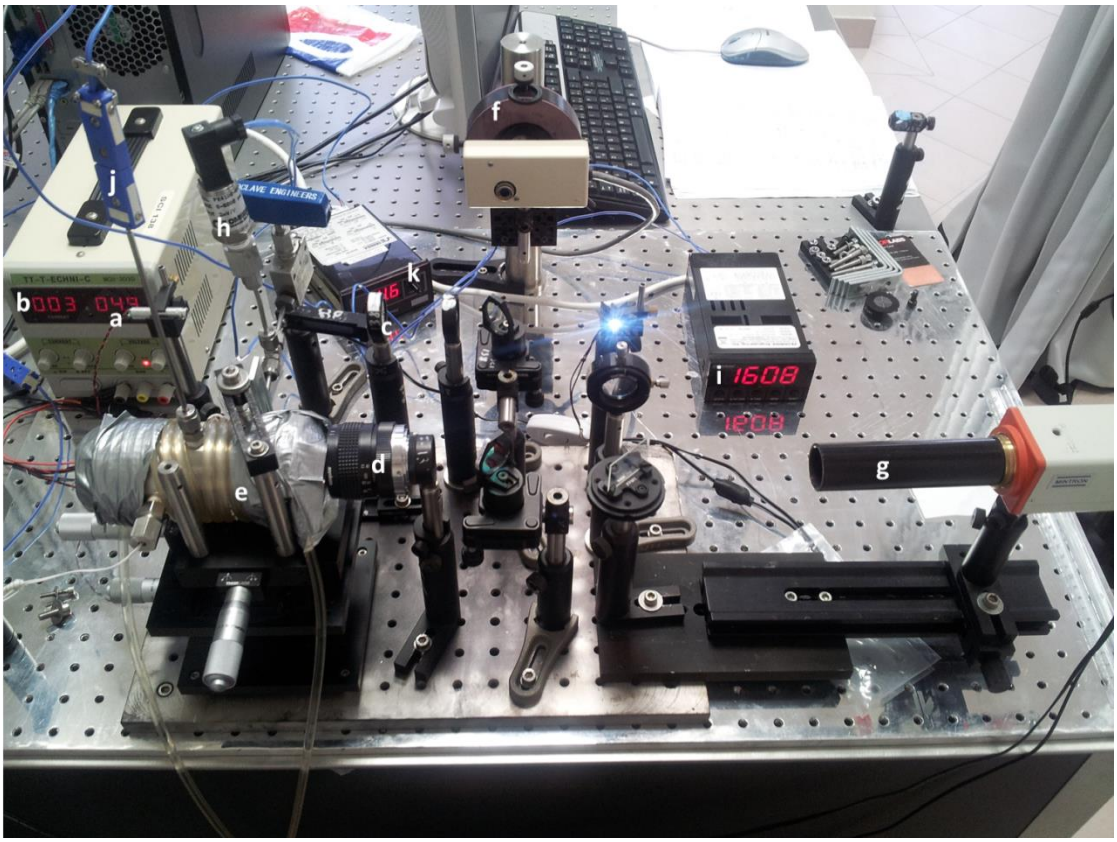

Figure 3.3. The experimental setup. Optical Components (a) A near-infrared laser beam (wavelength 780 nm, maximal power 4.5 mW, CPS 192,Thorlabs) (b) TT-T-ECNIC MCH 303D Voltage supply (c) beam transformation telescope (d) Objective lens (e) TharSFC 05424-4 High Pressure Vessel (f) QPD (Quadrant Photodiode Detector) (g) Camera (h) Omega PX 4100 Pressure Transducer (i) Pressure Display Omega DP25B-S-230 (j) Omega T type Thermocouple (k) Temperature Display Omega DP462

3.2 Principle of Frequency Response Measurements

During measurements, ferromagnetic cantilevers were driven with a varying magnetic field generated by the coil due to a sinusoidal signal that was generated by a function generator, and subsequently amplified 50× by a high-voltage, high-frequency amplifier. The deflections of the driven cantilevers were detected by an AFM like scheme. A near-infrared laser beam was transformed with a telescope consisting of two identical lenses (f = 30 mm) and then focused on the cantilever surface with an objective. The beam reflected from the oscillating cantilever was detected with a quadrant photodiode (QPD). QPD is sensitive to the beam position within its surface and thus records the changes in the reflected beam due to cantilever deflection. The deflection signal together with the reference signal generated from the function generator was send to a lock-in-amplifier in order to improve the signal-to-noise ratio by detecting only the signals modulated at the actual driving frequency. Amplitude of the deflection and its phase shift with regard to the driving were detected by the lock-in amplifier and digitized using a data acquisition board controlled from Matlab programming environment

3.3 Componenets in the Measurement Setup

3.3.1 Microcantilever

Ferromagnetic cantilever made out of nickel with a length of approximately 200 μm, a width of approximately 20 μm, and a thickness about 1μm was used in this study. It was composed of three layers where chromium layer with a thickness of 10-20 nm was the bottom layer, gold layer of 100-200 nm was the middle layer, and nickel layer of 0.85-0.95 μm was on the top. The design and fabrication of these ferromagnetic microcantilevers were explained in detail in our previous study.[5] The schematic representation of the cantilever together with a micrograph of the actual device is shown in Figure 3.4.

Figure 3.4. (left) Schematic representation of microcantilever used for the fluid density and viscosity measurements (right) Micrograph of the microcantilever

3.3.2 High Pressure Vessel

A die with microcantilevers was mounted in a Teflon housing (see Figure 3.5) with an electromagnetic actuator - a coil made from Cu wire - and placed in a 50 mL cylindrical high-pressure vessel with two sapphire windows at each side (TharSFC 05424-4). These windows allowed both monitoring the cantilevers and frequency response measurements by laser beam deflection. The electrical connection to the actuator in the pressure vessel was sealed using insulated CONAX Technologies TG24 T gland assemblies. Plastic tubing was wrapped around the vessel and connected to a heating circulator (Polyscience) to provide temperature control. Temperature and pressure in the vessel was monitored throughout the experiment with a T-type thermocouple (Omega) with ±1 K accuracy and with a pressure transducer (Omega PX 4100) with ±0.03 MPa accuracy.

Figure 3.5. Microcantilevers mounted in a Teflon housing with an electromagnetic coil

3.3.3 Quadrant Photodiode

Quadrant photodiode used in the experiments consists of 4 independent quadrant shaped photodiodes separated by a small distance as shown in Figure 3.6. It is sensitive to the position of the incident laser beam within its surface and provides two dimensional measurements in horizontal and/or vertical directions. When an incident beam with enough energy impinges on the depletion region of the semiconductor diode, it releases electron from the atomic structure. This produces a free electron(-) and a hole(+). If an external electric field is applied, electrons will be pulled out and current through the diode will change. Thus the photocurrent will be produced by each segment (Q1,Q2,Q3,Q4).

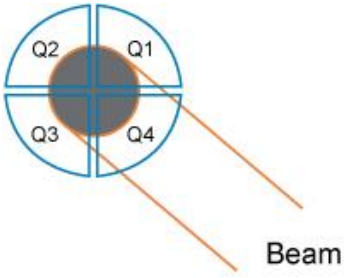

Figure 3.6. Schematic presentation of Quadrant Photodiode

The two-dimensional position signal can be then calculated as the difference between the left and right halves of the photodetector (x-axis) and the top and bottom halves of the photodetector (y-axis):

X= (Q2+Q3)-(Q1+Q4)

Y=(Q1+Q2)-(Q3+Q4)

The signals (X, Y) are detected using A/D converter [39]. Before measurements, the laser beam is centered on the sensor (X,Y)=(0,0)

3.4 Measurement Procedure

Nitrogen, argon and carbon dioxide were supplied by Aligaz Messer with purities of 99.9 %,99.5% and 99.9 %, respectively.

In the beginning of each set of measurements, the vessel was filled with desired fluid or fluid mixture to a pressure between 23 and 24 MPa with the syringe pump.

3.4.1 Fluid Transfer and Fluid Mixture Preparation

Fluids were transferred to the pressure vessel using a TELEDYNE ISCO D Series syringe pump (see Figure 3.6). Prior to the measurements with each fluid, the connecting lines and the vessel were flushed for several times with the studied fluid. Nitrogen was first filled to the pump and then brought to the maximal desired pressure. Subsequently, it was send to the sample chamber. On the other hand, carbon dioxide requires additional cooling step in order to maximize the mass supplied to the pump. As carbon dioxide was being transferred from a storage cylinder, the temperature of the pump was decreased to about 9 ºC. Then, inlet and outlet of the pump was closed and temperature was increased to the room temperature. Carbon dioxide was brought to desired maximal pressure and sent to the sample chamber.

Mixture preparation requires successive transfer of fluids, CO_2 and N_2, to the sample chamber where the amount of each fluid was determined via mass measurements to have a desired composition. First, the mass of empty sample chamber was measured and recorded. In order to determine which fluid should be transferred first to the chamber, the densities of each fluid at the maximal pressure(~23 MPa) were found from NIST database as 900 kg/m^3 and 200 kg/m^3 for CO_2 and N_2, respectively [9]. The volume of the sample chamber is constant and known; mass of each fluid was calculated from the density and volume. For carbon dioxide, higher masses can be obtained at lower pressures; therefore CO_2 was first introduced to the chamber. The amount of carbon dioxide introduced was calculated from the difference of the actual weight and the weight of an empty chamber. Subsequently, amount of nitrogen that should be added to the chamber was calculated according to the desired composition. Nitrogen filling

requires several attempts to get a mixture whose composition results to be close enough to the desired one. All mass measurements were done with a mass balance with an accuracy of ± 0.1 g and the compositions were calculated with ± 0.01 accuracy.

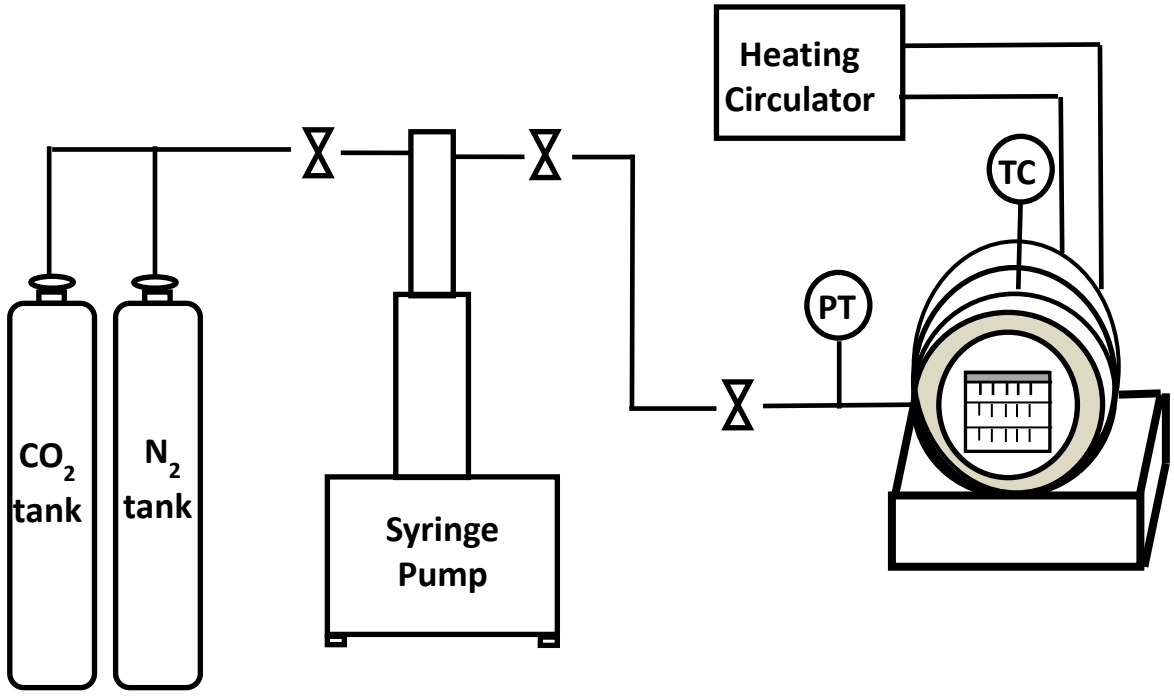

Fig.3.7: Schematic of the system for the sample chamber pressurization

After the vessel is filled with the fluid to the highest pressure; then the temperature of the vessel was adjusted to the desired temperature by heating circulator. Stable pressure and temperature of the system was reached in about 1-2 hours. Subsequently, frequency response measurements were performed beginning from the highest pressure and then the pressure was decreased step by step for successive measurements in the set. Temperature was kept constant throughout the measurements. At each pressure, driving frequency of the function generator was adjusted over a range of 9 kHz approximately centered on resonant frequency where 400 evenly distributed points were taken within the range. The amplitude of the driving sinusoidal signal was set to 3 V peak to peak.

According to Sader, the oscillation of an elastic cantilever beam can be approximated as a simple damped harmonic oscillator in the limit of small dissipation [25]. Therefore, the dissipation-free cantilever resonant frequency ω_{fluid} and the quality factor Q were determined by fitting the fundamental measured resonance peak to Eq. (3.1) which describes the motion of

simple damped harmonic oscillator . The derivation of the equation was shown in the previous section (see Eq. 2.28).

$$A(\omega) = \frac{A_0 {\omega_{fluid}}^2}{\sqrt{({\omega^2 - {\omega_{fluid}}^2})^2 + \frac{\omega^2 {\omega_{fluid}}^2}{Q^2}}} \tag{3.1}$$

where A_0 is the zero-frequency amplitude of the response and ω is the angular driving frequency. At each pressure, three measurements were taken and then averaged to obtain representative value at the given fluid pressure and temperature. The mean value of the relative standard deviation of resonant frequency and Q-factor measurements was 0.1% and 3.4%, respectively, while the maximum deviations were 0.7% and 13.4%, respectively.

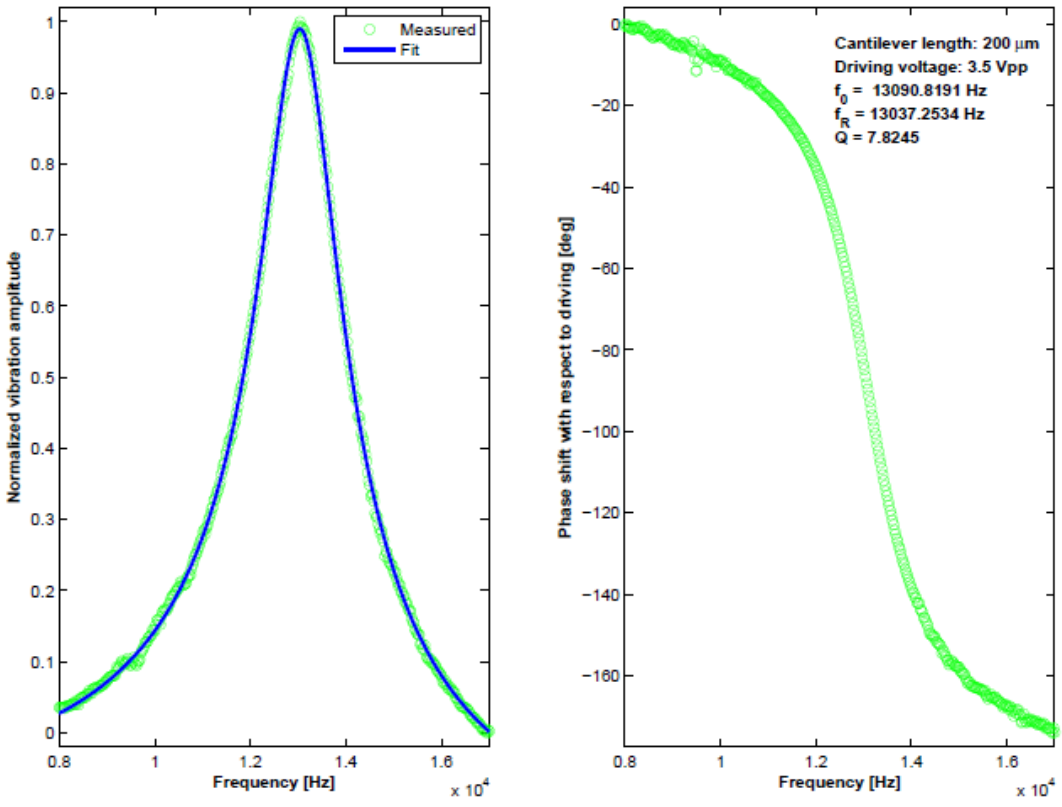

Figure 3.8: Cantilever frequency response at 308.15K and 12.5 MPa with CO_2

3.4.2 Decane Measurement

Decane was transferred to the vessel using a glass pipette under the hood. No pressurization was performed since measurements were performed at atmospheric pressure. Removing decane from the sample vessel was different than the cleaning of nitrogen, argon and carbon dioxide. Cleaning procedure was done with supercritical carbon dioxide more than 6 times to ensure complete removal of decane from the vessel. First of all, most of decane was removed by pouring the decane to the closed container after the one of the sapphire window was opened. Subsequently, thermocouple was taken out and a new line was connected to the vessel in order to obtain a flow of supercritical carbon dioxide to remove remaining decane properly. The vessel was heated to about 318.15 K and pressured to 12 MPa. Inlet and outlet of the vessel is left closed for 5 minutes and then the outlet is opened to take out the decane dissolved in supercritical carbon dioxide.

3.4.3 Measurement at Vacuum

Vessel was connected to the vacuum pump to perform measurements. The pressure was monitored by a vacuum gage.

Chapter 4

4. Results and Discussion

4.1. Measurement of density and viscosity of Nitrogen and Argon

4.1.1 Frequency response of cantilevers immersed in Nitrogen and Argon

The dissipation-free resonant frequency, $f_{fluid} = \omega_{fluid}/2\pi$, and Q-factor measured with a 200 μm cantilever immersed in N_2 and Ar at 308.15 K and pressures up to 24 MPa are given in Figs. 4.1 and 4.2. The decrease in the resonant frequency observed with increasing fluid pressure can be attributed to the increase in the fluid mass moving along with the cantilever due to an increase in the fluid density with the pressure. Moreover, the effective volume of the fluid that is affected by cantilever oscillations increases with the fluid viscosity; thus, the increase of viscosity with increasing pressure contributes further to the decrease of the cantilever resonant frequency. Increase in viscosity also causes an increase in viscous damping and energy dissipation which translates into a decrease in the Q-factor value as pressure increases. The resonant frequency changes smoothly with pressure within the studied pressure range, including the phase transition pressures where a transition from supercritical to gaseous phase occurs. This behavior is a result of smooth changes of the fluid density and viscosity with fluid pressure for operating temperature well above the fluid critical point ($T_C = 126.2$ K for N_2 and $T_C = 150.7$ K for Ar). Q-factor for both fluids follows a similar behavior, a uniform decrease with pressure. The rate of the decrease in Q-factor is more pronounced at lower pressures

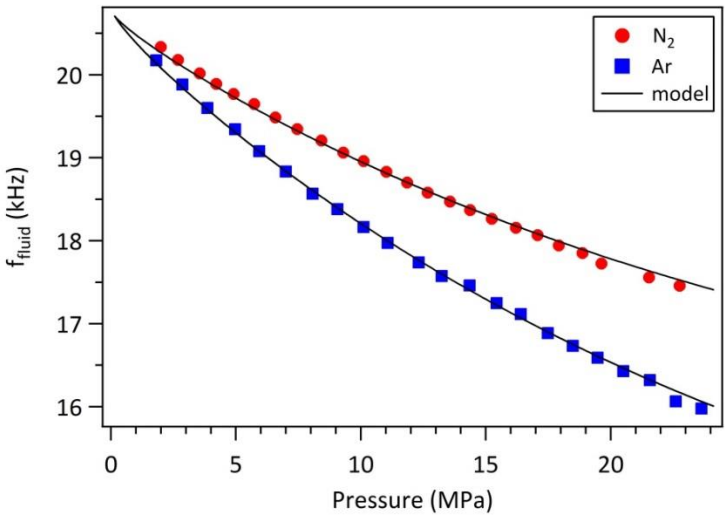

Fig. 4.1. Resonant frequency f_{fluid} of a driven microcantilever determined in N_2 and Ar at 308.15 K. Symbols: experimental data points, solid lines: fit of experimental data to Eq. (2.3)

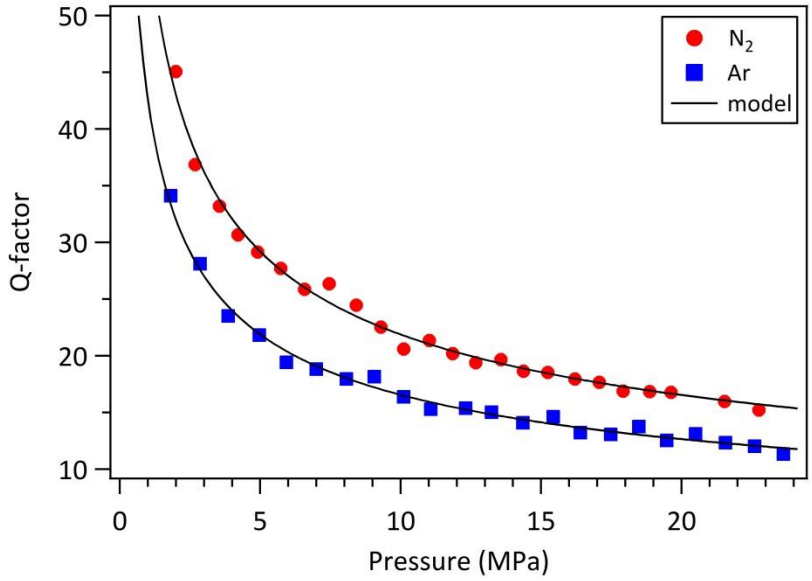

Fig. 4.2. Q-factor of a driven microcantilever determined in N_2 and Ar at 308.15 K. Symbols: experimental data points, solid lines: fit of experimental data to Eq. (2.4

In order to test the validity of Maali's approximation to Sader's hydrodynamic model of the immersed cantilever motion [25], experimental values of the cantilever angular resonant frequency, $\omega_{fluid,exp,i}$ and Q-factor, $Q_{exp,i}$ were fitted to model equations (2.3), (2.4) by minimizing the objective function F given by:

$$F= \sum_i \left\{ \left(\omega_{fluid,exp,i} - \omega_{vac} \left[1 + \frac{\pi \rho w}{4 \rho_c t} \left(1.0553 + 3.7997 \sqrt{\frac{2\mu}{\rho \omega_{fluid,exp,i} w^2}} \right) \right]^{-1/2} \right)^2 + \left(Q_{exp,i} - \frac{\frac{4\rho_c t}{\pi \rho w} + \left(1.0553 + 3.7997 \sqrt{\frac{2\mu}{\rho \omega_{fluid,exp,i} w^2}} \right)}{3.8018 \sqrt{\frac{2\mu}{\rho \omega_{fluid,exp,i} w^2}} + 2.7364 \frac{2\mu}{\rho \omega_{fluid,exp,i} w^2}} \right)^2 \right\} \quad (4.1)$$

The three parameters which were the vacuum resonant frequency (ω_{vac}), cantilever density $\times$ thickness ($\rho_c \times t$), and cantilever width (w) were regressed from the experimental data. To this end, density and viscosity values for both fluids required for the fitting were obtained from NIST Chemistry webbook [40]. As shown in Figs. 4.1 and 4.2, a very good agreement between the model and the experimental data was observed for both studied fluids. The fitted parameters ($\rho_c \times t$, w_{vac}, w) summarized in Table 4.1 are very similar for both fluids. This is expected since the cantilever properties should be independent of the type of fluid. An independent verification of the values of the fitted parameters was obtained from direct experiments and calculations. The width of the cantilever was measured with optical microscopy as 19.6 μm. From the cantilever frequency response recorded in evacuated high-pressure vessel (residual pressure 7 Torr), the vacuum resonant frequency was determined to be 20708 Hz which corresponds to the vacuum angular resonant frequency of 130112.2 rad/s. Cantilever density $\times$ thickness was calculated as 0.011 kg/m^2 by multiplying the average density of the cantilever by the total thickness of the cantilever. The average density of the cantilever was calculated using:

$$\rho_c = \frac{\sum_{i=1}^{3} V_i \rho_i}{\sum_{i=1}^{3} V_i} \tag{4.2}$$

where ρ_i and V_i is the density and volume of each layers of the microcantilever.

These values are close to the values regressed from the experimental data and show that Sader's model captures very well the physics of the immersed cantilever oscillations.

Table 4.1. Fitted calibration parameters for the studied cantilever

Fitted parameter	**N_2**	**Ar**	**Relative Difference of N_2 and Ar parameter values $100 * (N_2 - Ar)/N_2$ [%]**
$\rho_c \times t$ (kg/m^2)	0.0111	0.0109	1.8
w_{vac} (rad/s)	130627.4	130841.1	0.2
w (μm)	18.8	19.0	1.0

4.1.2.Determination of Densitiy and Viscosity of Nitrogen

This result suggests it should be possible to use the cantilever frequency response to measure simultaneously the density and viscosity of the immersion fluid. To that end, Eq. (2.3) and (2.4) can be re-written in the following form:

$$\omega_{fluid,exp} - \omega_{vac}\left[1 + \frac{\pi\rho w}{4\rho_c t} * \left(1.0553 + 3.7997\sqrt{\frac{2\mu}{\rho\omega_{fluid,exp} w^2}}\right)\right]^{-1/2} = 0 \tag{4.3}$$

$$Q_{exp} - \frac{\frac{4\rho_c t}{\pi\rho w} + \left(1.0553 + 3.7997\sqrt{\frac{2\mu}{\rho\omega_{fluid,exp} w^2}}\right)}{3.8018\sqrt{\frac{2\mu}{\rho\omega_{fluid,exp} w^2}} + 2.7364\frac{2\mu}{\rho\omega_{fluid,exp} w^2}} = 0 \tag{4.4}$$

At a certain fluid temperature and pressure, the cantilever angular resonant frequency $\omega_{fluid,exp}$ and quality factor Q_{exp} are measured and inserted into Eq. (4.3) and (4.4) together with the three cantilever calibration parameters $(\rho_c \times t,\ \omega_{vac}, w)$. Subsequently, the density and viscosity of the studied fluid satisfying simultaneously Eq. (4.3) and (4.4) can be found using an appropriate numerical method.

As described above, cantilever calibration parameters can be in principle determined independently using different instruments. However, due to the variations in the cantilever manufacturing process, this characterization must be generally done for each individual cantilever, which is neither easy nor convenient. Moreover, cantilever dimensions and elastic modulus change with temperature[5]. In order to estimate the influence of errors in the cantilever calibration parameters on the measured values of fluid density and viscosity, we calculated the deviations in the measured density and viscosity of Ar due to the deviations in these three parameters $(\rho_c \times t,\ \omega_{vac}, w)$ from their true values. A 1% deviation in an individual calibration parameter was introduced (keeping the other two parameters constant) and then the change in the density and viscosity of Ar was calculated. The results of these calculations are summarized in Figs. 4.3 and 4.4. While the density and viscosity are fairly insensitive to deviations in $(\rho_c \times t)$ and w, a 1% error in ω_{vac} leads to large systematic deviations in the calculated values of density and viscosity (ρ_{calc}, μ_{calc}) with respect to the expected values (ρ_{NIST}, μ_{NIST}) determined from the NIST reference data [9].

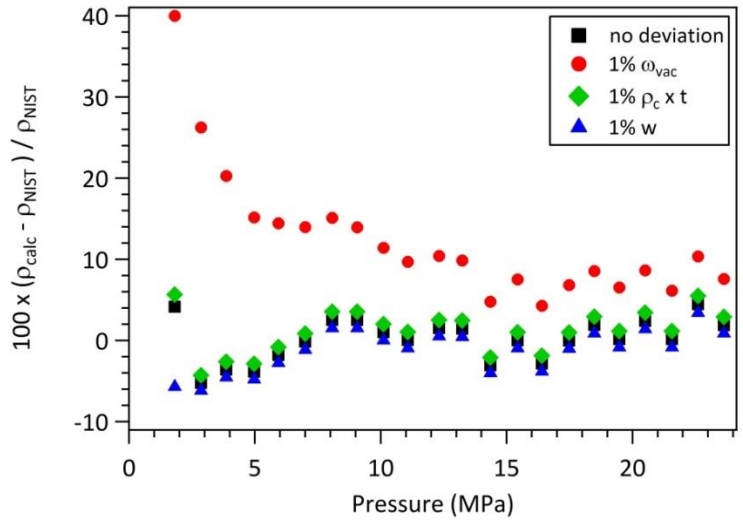

Fig. 4.3. The effect of errors in the cantilever calibration parameters on the relative error of density of Ar at 308.15 K.

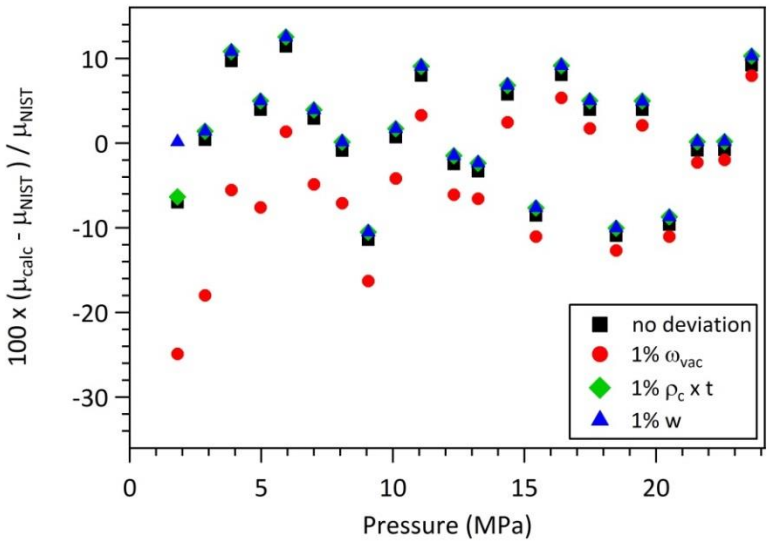

Fig. 4.4. The effect of errors in the cantilever calibration parameters on the relative error of viscosity of Ar at 308.15 K.

As an alternative to the direct measurement or calculation, cantilever calibration parameters can be determined from a series of frequency-response measurements in a reference fluid with density and viscosity known very accurately for each individual measurement in the series. This way, one does not need to know the exact details about the composition, geometry or any mechanical properties of the cantilever, since this information can be obtained from experimental data by regression. We adopted this approach with Ar as the reference fluid and determined the density and viscosity of N_2 using the cantilever calibration parameters regressed from the frequency response data of Ar. The deviations of the calculated density and viscosity of N_2 (ρ_{calc}, μ_{calc}) from the values (ρ_{NIST}, μ_{NIST}) obtained from the NIST database are presented in Figs. 4.5 and 4.6. As illustrated by these figures, no systematic deviation of the measured and expected values is observed for both density and viscosity and their error is randomly scattered about the zero value. The root-mean-square deviation of density and viscosity were 2.5% and 5.2% in the studied pressure range while the maximum deviations were below 4.9% and 11.4%, respectively.

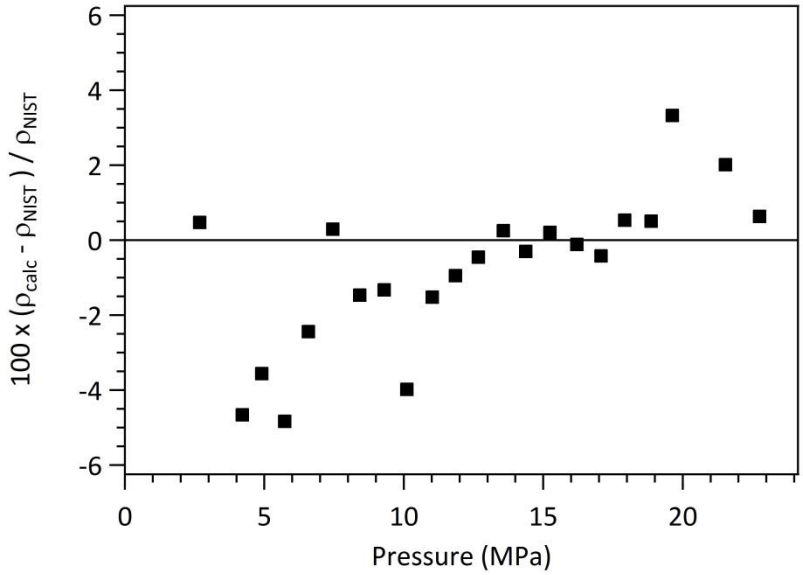

Fig. 4.5. Relative deviation of the measured density of N_2 from the expected values. Experimental values of N_2 density were calculated using Ar as the reference fluid.

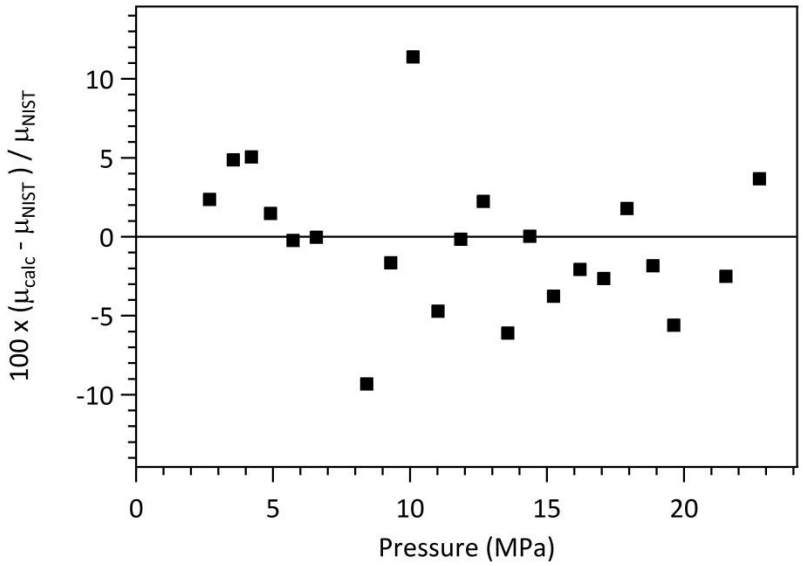

Fig. 4.6. Relative deviation of the measured viscosity of N_2 from the expected values. Experimental values of N_2 viscosity were calculated using Ar as the reference fluid.

These results are very promising and show the potential of the technique for accurate, simultaneous measurements of the fluid viscosity and density. From the comparison of Figs. 4.5 and 4.6, it follows that density could be measured with a higher precision compared to viscosity. One possible reason is that the resonant frequency can be determined more precisely from the measured frequency responses than the Q-factor. Relative standard deviation of the resonant frequency given by (standard deviation/average*100) was lower than that of the Q-factor for the measurements with both fluids at the studied pressure range. In particular, the average relative standard deviations of the resonant frequency and the Q-factor in all N_2 and Ar experiments were 0.1% and 3.6%, respectively. Inspection of model equations (2.3) and (2.4) reveals that the resonant frequency ω_{fluid} depends only weakly on the fluid viscosity ($\omega_{\text{fluid}} \propto \mu^{-1/4}$) whereas the dependence of the Q-factor on viscosity is much stronger (leading term of $Q \propto \mu^{-1/2}$). Thus, in solving coupled Eq. (4.3) and (4.4) for the fluid density and viscosity, contribution of experimental values of the Q-factor to the calculated viscosity is more important than the contribution of measured resonant frequencies. Higher error in the measured Q-factor values then results in less precise viscosity values. On the other hand, leading terms of both ω_{fluid} and Q depend on the fluid density as $\propto \rho^{-1/2}$. Consequently, measured values of ω_{fluid} and Q contribute approximately equally to the measured density values and the effect of random error caused by high variations of the Q-factor is somewhat reduced by more precise measurements of ω_{fluid}.

4.2. CO_2,N_2 and CO_2-N_2 Binary Mixture Measurements

In our previous study [5], we performed frequency response measurements with pure CO_2 at pressures up to 27 MPa with a custom-built experimental setup. A good agreement between experimental data and Sader's model was observed, which suggested that the fluid density and viscosity could be measured simultaneously at high pressures. In

section 4.1, we presented measurements of density and viscosity of N_2 at pressures up to 24 MPa using argon as reference fluid. The root-mean-square deviations of the measured density and viscosity of N_2 from the reference values obtained from NIST database were 2.5% and 5.2%. The experimental results obtained in our studies motivate us to investigate the thermophysical properties density and viscosity of fluid mixtures at high pressure.

4.2.1 Frequency response of microcantilever immersed in CO_2,N_2 and CO_2-N_2 Binary Mixture

Dissipation free resonant frequency f_{fluid} and Q-factor were measured for CO_2, N_2, and mixtures of CO_2 and N_2 at 35 °C with 200 μm length cantilevers from atmospheric pressure to 23MPa. Fig.4.7 and Fig.4.8 show that the resonant frequencies and Q-factors are decreasing with the increasing pressure for all studied mixture compositions. The resonant frequency decreases due to added mass moving along with the cantilever due to the increase in density with increasing pressure. The effective volume of the fluid that is affected by cantilever oscillations increases with the fluid viscosity; thus, the increase in viscosity with increasing pressure further decreases the cantilever resonant frequency. The increase in viscosity causes higher drag force and thus decreases Q factor. However, the magnitude of decrease in the resonant frequency and quality factor curves is not identical for different compositions of CO_2 – N_2 mixture. A more substantial change occurs in the resonant frequency and quality factor for pure CO_2 since the operating temperature 308.15 K is close to the critical temperature of CO_2. In the proximity of phase transition point, change in pressure results in a dramatic change in the density and viscosity and, thus, a dramatic change in resonant frequency and quality factor. As nitrogen molar fraction in the CO_2 – N_2 mixture increases, slope for both curves decreases because the studied

temperature and pressure range was much higher than the critical temperature and pressure of nitrogen.

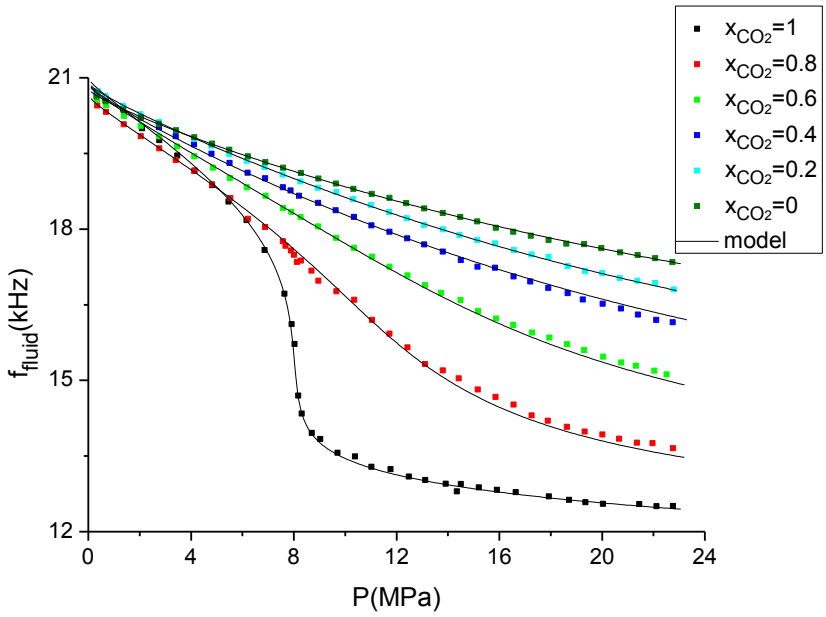

Fig. 4.7. Resonant frequency of a driven microcantilever determined in N_2-CO_2 binary mixture at 308.15 K. Symbols: experimental data points, solid lines: fit of experimental data to Eqs. (2.3)-(2.4)

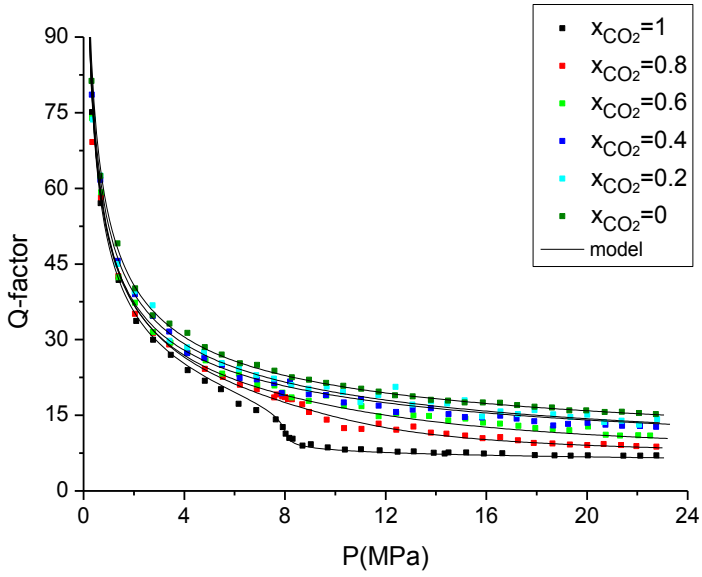

Fig. 4.8. Q-factor of a driven microcantilever determined in N_2-CO_2 binary mixture at 308.15 K. Symbols: experimental data points, solid lines: fit of experimental data to Eqs. (2.3)-(2.4)

Experimental data was analyzed using Sader's model. Using the known density and viscosity, experimental values of the cantilever angular resonant frequency, $\omega_{fluid,exp,i}$ and Q-factor, $Q_{exp,i}$ were fitted to model equations (2.3), (2.4) at the studied pressure range and fit parameters $(\omega_{vac}, \rho_c \times t, w)$ were obtained by minimizing the objective function F given in Equation 4.1.

Density and viscosity values for pure CO_2 and pure N_2 were determined from NIST Chemistry webbook [9] while the density of a given CO_2 –N_2 Binary mixture was predicted from Gerg equation of state [6]. The choice of the Equations of State (EoS) to calculate the density is based on two main factors. The first one is how much an EoS is suitable for determining the density of gas and the supercritical fluids at a wide range of pressures and

the studied temperature. The second one is the availability (accessibility) of the model equations and coefficients, exponents or constant parameters for calculating the density of CO_2 - N_2 mixture. Soave-Redlich-Kwong and Peng-Robinson EoS were also used to calculate density and the values were compared with NIST database for pure N_2 and CO_2, and some experimental studies also measured the density of CO_2 –N_2 mixture [41, 42]. However, the density values using these EoS were not as accurate as values obtained from Gerg EoS for CO_2 –N_2 Binary mixture at high pressures. The typical deviation between the experimental density values of Seitz et al.[6] and the GERG-2008 is within 0.5 % to 1 % range and which agrees well with the assumed uncertainty of the measurements

The Gerg EoS predict density accurately for a wide range of temperatures (from 90 to 450 K) and pressures (up to 35 MPa) involving the gas, liquid and supercritical region for mixtures.

Density of CO_2 –N_2 Binary mixture was calculated using Eq. 4.5:

$$\frac{p\,(\delta,\tau,\bar{x})}{\rho RT} = 1 + \delta\alpha_{\delta}^{r} \tag{4.5}$$

where p is the pressure, ρ is the density, T is the temperature, δ is the reduced mixture density, τ is the inverse reduced mixture temperature, $\bar{x}$ is the molar composition and α_{δ}^{r} is the residual part of the reduced Helmholtz free energy of the mixture. The equations for δ and α_{δ}^{r} were provided by Kunz and Wagner [6].

Viscosity of the CO_2-N_2 mixture was calculated using Chung Equation which is commonly used for both polar and nonpolar dense gas mixtures [43]. Theoretical correlations that predict the viscosity of gas mixtures at high pressures are limited. Viscosity of CO_2-N_2 mixture was calculated using both Lucas Equation [ref] and Chung Equation, and compared with two experimental studies which measured viscosity at varying pressure 20-120 bar, temperature 289-293 K and a composition of 0.38-0.50 carbon dioxide [44, 45]. Chung equation predicts viscosity better than Lucas equation

especially at high pressures and the relative deviation with these experimental studies did not exceed 4%. Chung equation requires density and temperature as input; thus density predicted by Gerg EoS was used. Viscosity was calculated using Eq. 4.6:

$$\mu = \mu^* \frac{36.344(MT_c)^{1/2}}{V_c^{2/3}} \quad (4.6)$$

where μ is the viscosity, M is the molecular weight, T_c is the critical temperature, V_c is the critical volume. The equation for μ^* was given in Reference [43]. Moreover parameters T_c, V_c and M in the equation were given as functions of mixture composition.

The comparison of experimental data with the Sader's Model is shown in Fig. 4.7 and Fig.4.8 for pure CO_2, pure N_2, and four different compositions of CO_2-N_2 mixture by minimizing the function F as described above. A good agreement is observed between the models and measurements.

Table 4.2 shows the summary of fitted parameters regressed from the experimental data for different compositions of CO_2-N_2 mixture .The fitted parameters values are close for different compositions, as the cantilever properties are independent of the composition of fluids.

Table 4.2: Fitted parameters for the studied cantilever

Fit Parameters/composition	$y_{CO_2} = 1$	$y_{CO_2} = 0.8$	$y_{CO_2} = 0.6$	$y_{CO_2} = 0.4$	$y_{CO_2} = 0.2$	$y_{CO_2} = 0$
$\rho_c \times t$ (kg/m2)	0.01032	0.0106	0.01027	0.01015	0.01034	0.01051
f_{vac} (Hz)	21007.3	20672.4	20884	20903.6	20919.4	20794.1
w (μm)	20.16	20.80	20.26	21.00	19.50	19.17

The fitted parameter values given in Table 4.2 are compared to the values obtained by independent experiments and calculations. The fitted parameters values are close to the directly measured values which shows that Sader's model is also validated for mixtures.

The relative difference between the calculated resonant frequency($\omega_{fluid,calc}$) and Q-factor (Q_{calc}) and the experimental resonant frequency ($\omega_{\text{fluid,exp}}$) and Q-factor ($Q_{\text{exp}}$) was determined at each studied pressure as follows. First $\omega_{fluid,calc}$ and Q_{calc} were calculated by inserting three fitted parameters together with density and viscosity to Eqs (4.7)-(4.8) and solving these equations simultaneously. Subsequently, relative differences were determined from $(\omega_{fluid,calc} - \omega_{\text{fluid,exp}})/\ \omega_{fluid,calc} * 100$ and $(Q_{calc} - Q_{\text{exp}})/\ Q_{calc} * 100$. The resulting values are given in Tables 4.3-4.4.

$$\omega_{fluid,calc} - \omega_{vac} * [\,1 + \frac{\pi\rho w}{4\rho_c t} * \left(1.0553 + 3.7997\sqrt{\frac{2\eta}{\rho\omega_{fluid,calc}\, w^2}}\right)\,]^{-1/2} = 0 \qquad (4.7)$$

$$Q_{calc} - \frac{\frac{4\rho_c t}{\pi\rho w} + (1.0553 + 3.7997\sqrt{\frac{2\eta}{\rho\omega_{fluid,calc} w^2}})}{3.8018\sqrt{\frac{2\eta}{\rho\omega_{fluid,calc}\, w^2}} + 2.7364\frac{2\eta}{\rho\omega_{fluid,calc} w^2}} = 0 \qquad (4.8)$$

Table 4.3: Relative resonant frequency differences for CO_2- N_2 binary mixture

Relative percent difference/composition	$\mathbf{y_{CO_2} = 1}$	$\mathbf{y_{CO_2} = 0.8}$	$\mathbf{y_{CO_2} = 0.6}$	$\mathbf{y_{CO_2} = 0.4}$	$\mathbf{y_{CO_2} = 0.2}$	$\mathbf{y_{CO_2} = 0}$
Average	0.39	0.57	0.40	0.26	0.09	0.07
Max	2.45	1.22	0.85	0.87	0.36	0.26

Table 4.4: Relative Q-factor differences for CO_2 - N_2 binary mixture

Relative percent difference/composition	$y_{CO_2} = 1$	$y_{CO_2} = 0.8$	$y_{CO_2} = 0.6$	$y_{CO_2} = 0.4$	$y_{CO_2} = 0.2$	$y_{CO_2} = 0$
Average	3.89	3.81	4.49	4.37	3.55	1.28
Max	9.95	12.70	14.20	10.43	16.26	4.60

4.2.2 D Determination of density and Viscosity of CO_2 ,N_2 and CO_2-N_2 Binary Mixture

As shown in Table 4.3 and 4.4, the relative difference between the experimental and theoretical resonant frequency and Q-factor is low. This result suggests it can be possible to use the cantilever frequency response to measure the density and viscosity of the desired fluid. To verify this hypothesis, density and viscosity of CO_2, N_2 and their mixture was calculated using frequency response and fit parameters. Fit parameters were determined from a set of measurements at a constant temperature using a reference fluid. Nitrogen was used as a reference fluid since its density and viscosity is accurately known and the experimental resonant frequency and quality factor agrees very well to the model. Moreover, it is cheap, inert and available. Subsequently, resonant frequency and Q-factor of the studied fluid measured at a certain temperature and pressure were inserted into equations 4.3 and 4.4 together with the fit parameters obtained from measurements with nitrogen. Density and viscosity were obtained by solving these two equations simultaneously by numerical methods. Table 4.5 shows the relative difference between the measured density and viscosity values and the theoretical values obtained from Gerg EoS and Chung Equations for CO_2 –N_2 Binary mixtures. Pure CO_2 and N_2 density and viscosity values were compared with NIST reference data. As shown in the table, relative differences are higher when carbon dioxide is used as reference fluid.

Table 4.5. Relative difference between the measured and predicted density and viscosity values of CO_2-N_2 binary mixture at 35 C temperature and 0-23 MPa pressure

Relative percent difference	**Reference fluid**	$y_{CO_2} = 1$	$y_{CO_2} = 0.8$	$y_{CO_2} = 0.6$	$y_{CO_2} = 0.4$	$y_{CO_2} = 0.2$	$y_{CO_2} = 0$
Average density	$C0_2$	2.46	14.83	7.6	11.4	3.65	9.33
Max density		13.32	60.66	39.61	22.67	26.07	52.43
Average viscosity		8.18	15.26	11.25	8.6	7.73	6.87
Max viscosity		25.17	27.35	24.78	20.56	26.67	27.17
Average density	N_2	4.12	13.28	3.86	7.74	5.06	0.96
Max density		11.51	31.32	6.41	14.48	23.64	3.12
Average viscosity		11.85	15.2	9.7	6.58	9.18	2.43
Max viscosity		27.65	24.06	25.66	19.16	28.64	7.18

The average relative deviation range is 0.96 -13.27 for density, and 2.42- 15.19 for viscosity when nitrogen is used as reference fluid. The variation in the deviation is due to the sensitivity of our methodology to fit parameters. The measured density and viscosity are very sensitive to the value of the vacuum resonant frequency of the cantilever, as discussed in section 4.1 The small errors in in vacuum resonant frequency may result in large errors in measured values.

The temperature and pressure measurement in a controlled environment is very significant in this study. The CO_2 properties were investigated using CO_2 as reference fluid to check the sensitivity of the system to the precision of pressure measurement. In our previous study, pressure of the fluid was monitored with a pressure transducer (Omega PX 4100) with ±0.1MPa accuracy. In this study, a pressure transducer (Omega PX409-5.0KAUSBH) with ±0.03 MPa accuracy is used. The resonant frequency and Q-factor values obtained from measurements with Omega PX 410 and PX409-5.0KAUSBH

pressure transducers were compared for CO_2 fluid at a pressure range of 0-24 MPa and 308.15 K temperature. The average relative difference in resonant frequency and Q-factor was found 0.2 % and 1.1 % for CO_2 at pressures greater than 9 MPa respectively with PX-4100. The relative difference became 8% for resonant frequency and 20 % for Q at pressures close to the vicinity of the critical pressure of CO_2. While with the new transducer(Omega PX409-5.0KAUSBH), the relative average deviation in density and viscosity w.r.t NIST is reduced from 1.04 % to 0.80 % and 8.59% to 7.23 % respectively for pressures greater than 9 MPa. However, at pressures close to the vicinity of the critical pressure of CO_2 the relative average deviation in density and viscosity is reduced from 30 % to 11 % and 30 % to 16% respectively. The introduction of the new pressure transducer in the experimental setup has enhanced the precision of our system.

The operating temperature is 308.15 K and any small error in temperature readout affects the accuracy of the density and viscosity values. In order to estimate the effect of temperature measurement errors on the measured values of fluid density and viscosity, we calculated the deviations in the measured density and viscosity of $0.6C_2$ - $0.4N_2$ mixture at 307.15,308.15 and 309.15 K temperatures. One Kelvin change in temperature was introduced which is the accuracy of the thermocouple sensor used for measuring temperature. Fit parameters characterizing the cantilever were taken from the reference measurement at 308.15 K. The theoretical values of density and viscosity at 307.15,308.15 and 309.15 K were calculated using Gerg EoS and Chung equation. Subsequently, the experimental values of density and viscosity obtained at the nominal temperature of 308.15 K provided by temperature transducer were compared with the theoretical values. Figs. 4.9 and 4.10 show the relative deviation of density and viscosity with respect to the temperature at pressures up to 23 MPa. The change in the relative deviation in density is higher than viscosity. Relative difference of density and viscosity with respect to Gerg EoS and Chung Equation at temperature 308.15 K and 309.15 K is low compared to the 307.15

K. Change in the relative difference is higher between the 307.15 K and 308.15 K compared to the the difference between 308.15 K and 309. 15 K due to the fact that temperature 307.15 K is closer to the critical temperature of CO_2.

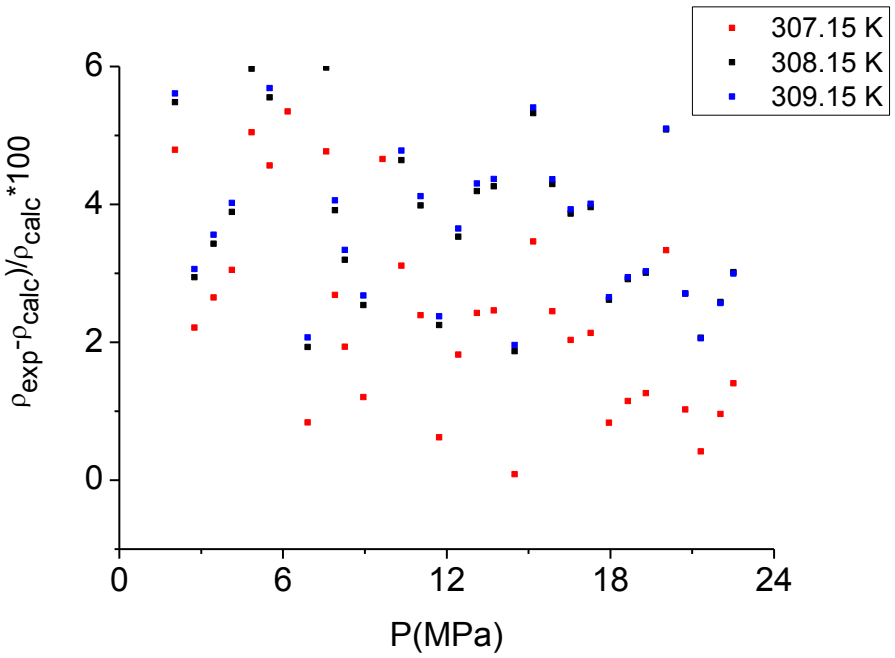

Fig.4.9. Relative density deviation at varying pressures at 307.15 K,308.15 K and 309.15 K temperature for 0.6CO.-0.4N_2 mixture

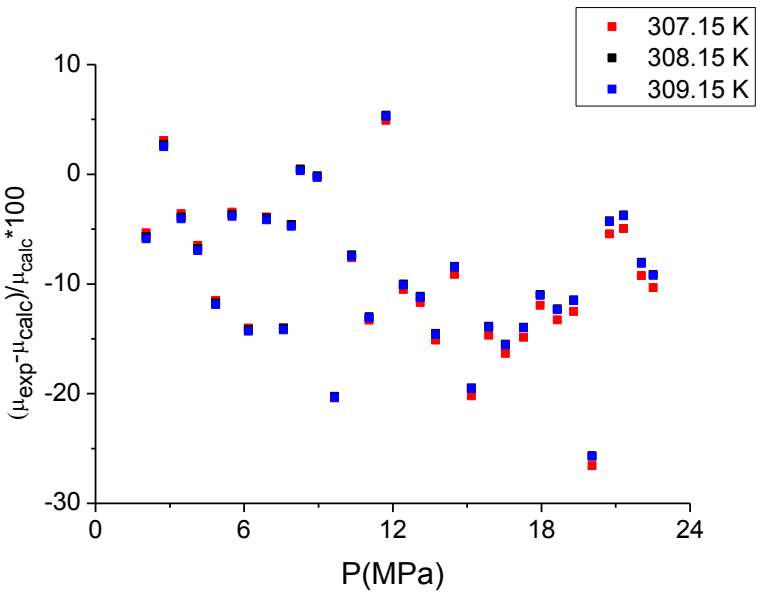

Fig.4.10. Relative viscosity deviation at varying pressures at 307.15,308.15 and 309.15 K for 0.6CO.-0.4N_2 mixture

4.2.3 Composition Determination of CO_2-N_2 Binary Mixture

As illustrated by Figures 4.7 and 4.8, the resonant frequency and Q-factor vary with different concentrations of CO_2-N_2 binary mixture at a constant temperature and pressure. Therefore, unknown concentration can be predicted when a calibration curve is constructed at known operating conditions. Fig. 4.11 shows the resonant frequencies at six different concentrations of CO_2-N_2 binary mixture, at four pressures and at 308.15 K. The resonant frequency decreases as the molar fraction of carbon dioxide increases due to increase in density and viscosity values. The reason is that change in the density and viscosity is bigger at higher carbon dioxide concentrations. The operating pressure range involves the vicinity of the critical pressure of carbon dioxide where a phase transition between vapor and

supercritical phase occurs and a dramatic change in the thermophysical properties is observed. As carbon dioxide concentration increases change in density and viscosity also increases which results in a more dramatic change in the resonant frequency. Therefore, using the approach suggested in this study, we can determine unknown concentration of binary mixtures. This approach can be used in carbon capture and storage process to remove impurities.

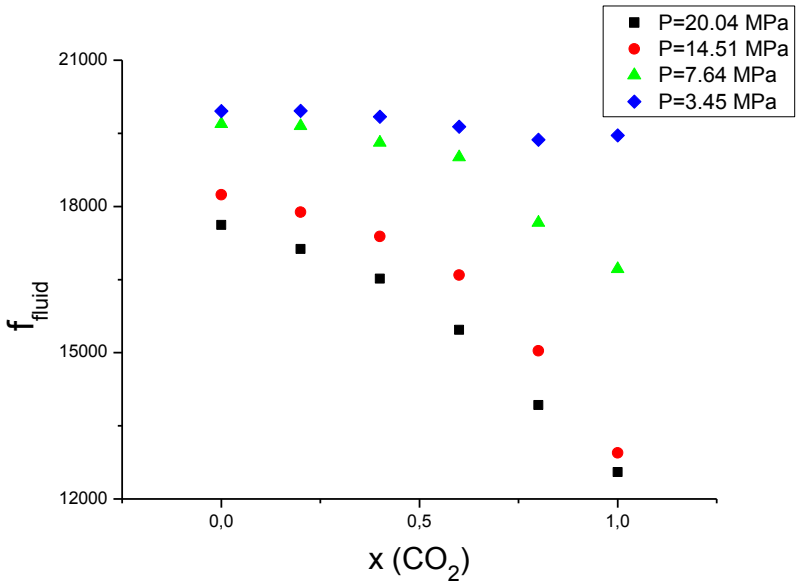

Fig.4.11. Variation of resonant frequency with composition of N_2-CO_2 binary mixture at different pressures and constant temperature of 308.15 K

4.3 Possible factors influencing Frequency Response Measurements

4.3.1 Effect of Adsorption of molecules on the Density and Viscosity Values

In general, it is possible that the fluid molecules might adsorb on the surface of the cantilever which would affect the resonant frequency and the Q-factor because of an increase in the mass of the cantilever due to the mass of the adsorbed molecules. This effect is not accounted for in Sader's model and, thus, it does not enter into the equations used to extract density and viscosity. Moreover, the effect of adsorption would not be constant in the pressure range investigated since the amount of adsorbed fluid molecules would increase with increasing pressure. In order to quantify the errors caused by this effect, we calculated the maximum amount of fluid that can be adsorbed on the surface of the cantilever assuming that the fluid molecules cover the surface as a tightly packed monolayer. For a cantilever with the total surface area of $8x10^{-9}$ m^2, the maximum amount of nitrogen that can be adsorbed is 2.3×10^{-12} g. We inserted the density and viscosity data of nitrogen to Eq. (4.3) and (4.4), together with the vacuum resonant frequency and the cantilever width, and used the two different values of $(\rho_c \times t)$ determined by including and excluding monolayer fluid adsorption, respectively. Subsequently, we calculated the resonant frequency and the Q-factor in order to relate the change in the cantilever mass to the changes in ω_{fluid} and Q. The calculation was performed for nitrogen at the highest pressure where ω_{fluid} and Q were the lowest. Resulting changes in ω_{fluid} and Q were found to be 0.01% and 0.04% which is much lower than the standard deviations in our measurements. Hence, we can conclude that the fluid adsorption has negligible effect on the determination of the fluid density and viscosity using the cantilever frequency response.

4.3.2 Effect of Heat Produced by Laser Beam on the Frequency Response

In general, it is possible that heat is produced on the cantilever since the laser beam is focused on the cantilever. This would cause increase in the temperature of cantilever and create a temperature difference between the cantilever and the surrounding fluid. Temperature difference would lead to convection in the fluid which may result errors in the resonant frequency and Q-factor values. Moreover, density and viscosity values in the vicinity of the cantilever could change due to localized heating. In order to investigate the errors caused by this effect, density filter was placed just in front of the laser to decrease its power to 0.7 mW. As shown in Table 4.6, the resonant frequency and Q-factor values measured with different laser power were found to be within the uncertainty of the measurements. Hence, we can conclude that the power of laser beam has negligible effect on the resonant frequency and Q-factor values and thus determination of the fluid density and viscosity using the cantilever frequency response.

Table 4.6 : f_{fluid} and Q-factor measurements with laser beam of two different power

Measurement/Power(mW)	4.2		0.7	
	f_{fluid}	Q	f_{fluid}	Q
1	17753.26	16.8042	17747.22	16.3278
2	17735.68	16.7458	17744.61	16.6371
3	17760.31	16.7628	17749.67	17.8501
Average	17749.75	16.77093	17747.17	16.93833
Standard Deviation	12.68717	0.030038	2.529614	0.804615
Relative Standard Deviation	0.071478	0.179105	0.014254	4.750261

4.3.3 Effect of Temperature on cantilever Calibration Parameters

When working within an extended range of fluid temperatures, stability of the microcantilever sensor calibration becomes an issue. As discussed by Uzunlar et al.[5], change in temperature ΔT affects the dimensions and elastic modulus of the cantilevers and, thus, calibration parameters $(\rho_c \times t,\ \omega_{vac}, w)$ also change. Cantilever linear dimensions (t, w) are proportional to $\sim(1 + \alpha\Delta T)$ which implies that the cantilever density ρ_c decreases with temperature as $\sim(1 + \alpha\Delta T)^{-3}$ where α is the coefficient of thermal expansion of the cantilever material. Similarly, elastic modulus of the cantilever changes as $\sim(1 + \beta\Delta T)$ where β is the coefficient of thermal dependence of the elastic modulus. Consequently, the vacuum resonant frequency ω_{vac} scales with temperature as $\sim(1 + \alpha\Delta T)^{0.5}(1 + \beta\Delta T)^{0.5}$. The magnitude of the temperature-induced changes of cantilever calibration parameters is given by the values of coefficients α and β and depends on the material of the cantilever. In order to avoid systematic errors in the measured values of density and viscosity, one-time calibration of the cantilever sensor with a reference fluid should be carried out at different temperatures within the range of interest. Subsequently, the calibration parameters for a particular experimental temperature can be determined by interpolation.

4.3.4 Limitations on the operating conditions

The high-pressure vessel used in our experiments imposes limitations on the accessible ranges of the fluid temperature and pressure (maximum temperature 150 ºC (423 K) and maximum pressure 6000 psi (41MPa), as specified by the manufacturer). These operating conditions can be further extended by using different high-pressure vessel designs. The frequency measurements with CO_2 and $0.8CO_2$-$0.2N_2$ were performed up to 27 MPa.

4.4.Measurement with Decane

In the previous sections, experiments with N_2, Ar, CO_2 and N_2-CO_2 mixture at 308.15 K and pressures up to 24MPa were carried out. This translates into the range of the fluid density and viscosity of 2-900 kg/m^3 and 18-90 μPa.s, respectively. However, the maximum values of density and viscosity (900 kg/m^3 and 90 μPa.s, respectively) obtained do not represent the upper limits of microcantilever-based measurements. In order to illustrate this point, frequency response of decane (726 kg/m^3 and 848.18 μPa.s) was measured at atmospheric pressure. Table 4.7 shows f_{fluid} and Q-factor measured at room temperature (R.T) and atmospheric pressure.

Table 4.7: f_{fluid} and Q-factor measurement of decane taken at R.T. and 1 atm

Measurement	**f_{fluid}**	**Q_{factor}**
1	11498.32	2.61
2	11470.14	2.67
3	11495.90	2.66
Average	11488.12	2.65
Standard Deviation	15.62	0.03
Relative Standard Deviation	0.14	1.13

.

The relative standard deviation of the Q-factor was found lower compared to previous measurements in gases and supercritical fluids/fluid mixtures. For example, the mean value of the relative standard deviation of Q-factor measurements at 0-24 MPa for N_2-CO_2 mixture at 308.15 K was 3.4% while the maximum deviation was 13.4%.

4.5 Measurements with cantilevers of varied length in CO_2 at 304.45 K

In order to study the effects of cantilever length on the sensitivity of density and viscosity measurements, dissipation-free resonant frequency f_{fluid} and Q-factor of cantilevers immersed in CO_2 were measured at 304.45 K for pressures up to 24 MPa with 200 µm, 300µm and 400µm cantilevers. As it is shown in figure 4.12 and 4.13, dissipation free resonant frequency and Q-factor were found to be decreasing with increasing pressure which is due to the increase in density and viscoisty. The slope of f_{fluid} with respect to the fluid pressure is higher for shorter cantilevers at any given range of pressure. This indicates that sensitivity of the frequency response to changing environmental conditions is higher for shorter cantilevers.

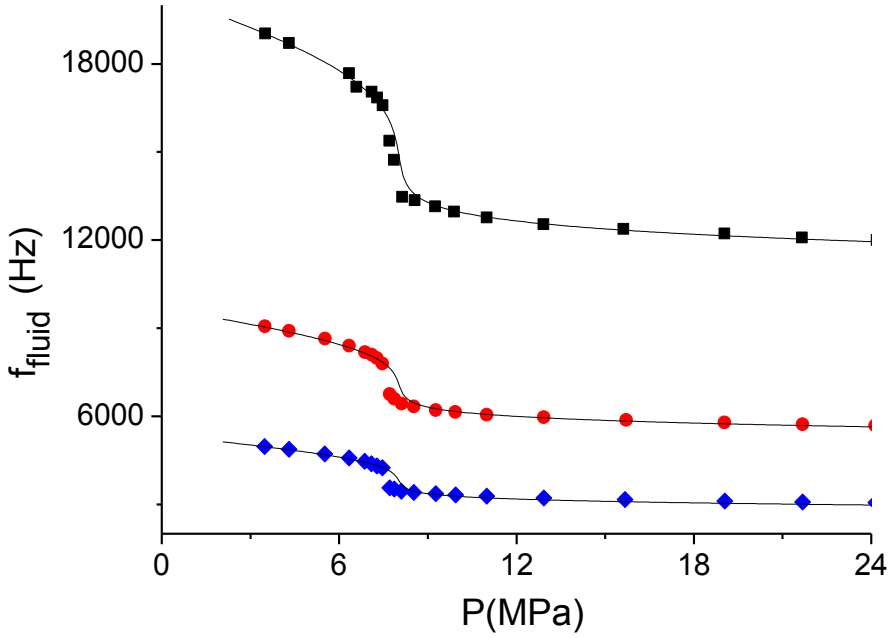

Fig. 4.12. Resonant frequency f_{fluid} of a driven microcantilever determined in CO_2 at 304.45 K for 200 µm (square), 300 µm (circle) and 400 µm (diamond) cantilevers. solid lines: fit of experimental data to Eq. (2.3)

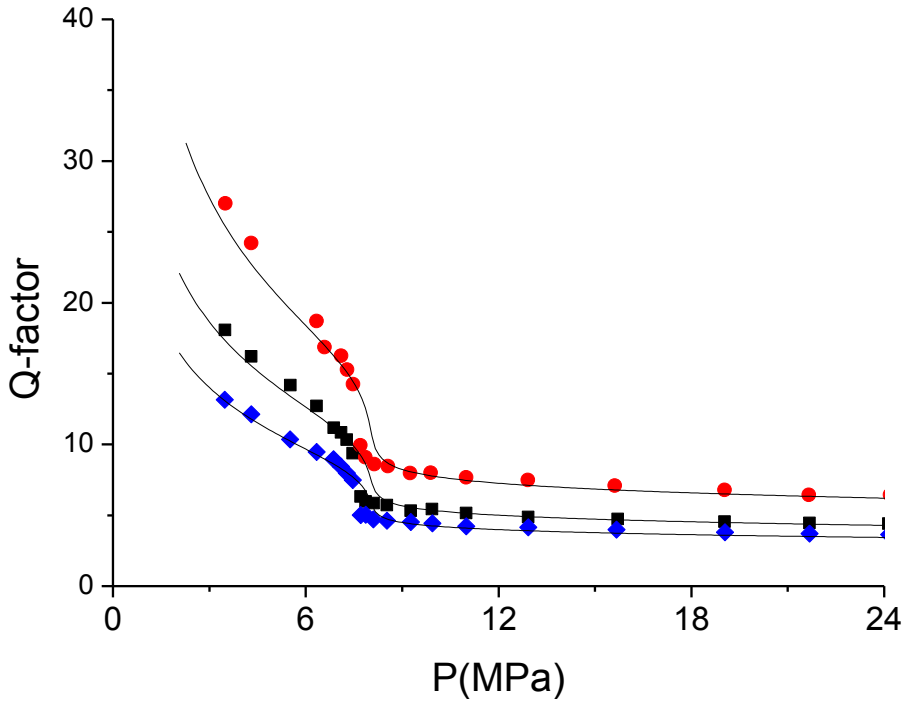

Fig. 4.13. Q-factor of a driven microcantilever determined in CO_2 at 304.45 K for 200 µm (square), 300 µm (circle) and 400 µm (diamond) cantilevers, solid lines: fit of experimental data to Eq. (2.4)

Chapter 5

CONCLUSION

5.1 Conclusion

In this thesis, we investigated the use of the measurements of the resonant frequency and Q-factor of ferromagnetic nickel microcantilever immersed in Ar, N_2, CO_2 and CO_2-N_2 binary mixtures at 308.15 K and pressures up to 24 MPa for simultaneous determination of fluid density and viscosity. Experimental data was analyzed using Sader's model which describes oscillatory motion of immersed cantilevers incorporating the effects of hydrodynamic forces. A very good agreement between the experimentally obtained cantilever resonant frequencies and quality factors and the predictions of Sader's model was observed. The low difference in experimental and theoretical values illustrates that our experimental approach is suitable for the density and viscosity measurement of supercritical fluids and fluid mixtures at wide range of pressures. We report on the simultaneous measurement of density and viscosity of nitrogen from the measured frequency responses of an oscillated microcantilever immersed in N_2. To this end, using argon as a reference fluid of known density and viscosity, cantilever calibration parameters were obtained from nonlinear regression of cantilever resonant frequencies and quality factors recorded in argon. Subsequently, these calibration parameters were used in the model equations to determine the density and viscosity of nitrogen at the given experimental pressure and temperature. In the studied pressure range, the root-mean-square deviations of the measured density and viscosity of nitrogen from the reference values obtained from NIST database were 2.5% and 5.2%, respectively. In order to investigate the density and viscosity of fluid mixtures, CO_2-N_2 binary mixture was chosen as a model fluid. The average relative deviation range for different compositions CO_2-N_2 binary mixture was found to be 0.96 % -13.27 % for density and 2.42 %- 15 % for viscosity when

N_2 is used as reference fluid. Moreover, measurements with decane were performed to investigate thefrequency reponse of high viscous fluids.

5.2.Suggestions for future work

1. Precise temperature control and measurement is very important in this study. A more accurate temperature measurement can be done with a thermistor (± 0.1 K) or Platinum Temperature Resistor (± 1 mK). The temperature control of sample chamber can be improved by designing a new sample chamber surrounded by a heating bath. This will reduce the sensitivity of fluid temperature to the outside temperature.
2. Using the small length cantilevers, the system sensitivity can be improved. A sensitive system will predict the density and viscosity properties of mixtures more accurately.
3. Since the measurements with cantilevers require very small sample volumes, compact and portable microcantilever-based sensors might enable continuous monitoring of chemical reactions in a fluid or physicochemical processes such as gelation or solidification in microfluidic applications at high temperatures and pressures by observing changes in density and viscosity.
4. The cantilevers can also be used as high-pressure sensors in microreactor systems for samples with constant density or composition.
5. Since the cantilever motion in the fluid is affected only by the fluid properties in the immediate vicinity of the cantilever, our experimental technique can be also applied to make localized measurements in binary phase (liquid-gas), tertiary phase (liquid-liquid-gas), or inhomogeneous systems.

REFERENCES

1. Pipitone, G. and O. Bolland, *Power generation with CO2 capture: Technology for CO2 purification.* International Journal of Greenhouse Gas Control, 2009. **3**(5): p. 528-534.
2. Wagner, W. and R. Kleinrahm, *Densimeters for very accurate density measurements of fluids over large ranges of temperature, pressure, and density.* Metrologia, 2004. **41**(2): p. S24-S39.
3. Wilhelm, J., et al., *A vibrating-wire viscometer for dilute and dense gases.* International Journal of Thermophysics, 1998. **19**(2): p. 391-401.
4. Tétin, S., et al., *Modeling and performance of uncoated microcantilever-based chemical sensors.* Sensors and Actuators B: Chemical, 2010. **143**(2): p. 555-560.
5. Jürgen Wilke, H.A., *Theory and Praxis of Capillary Viscometry Introduction.*
6. W. A.Wakeham, A.N., J.V. Sengers, *Measurement of theTransport Properties of Fluids.* Blackwell Scientific Publications for IUPAC: Oxford U.K., 1991.
7. D. S.Viswanath, T.G., D. H.Prasad,N. V.Dutt, K. Y.Rani,, *Viscosity of liquids: theory, estimation, experiment, and data.* Springer Science & Business Media, 2007.
8. *Adhesive Pre-cure Characterisation Viscometry*. Available from: http://www.adhesivestoolkit.com/Docs/test/Physical%20Analysis%20-%20Viscometry.xtp#ref4.
9. Schaschke, C.J., *High Pressure Viscosity Measurement with Falling Body Type Viscometers* International Review of Chemical Engineering 2010. **2**(5).
10. *Equıpment For Qualıty Control And R&D*. 2012; Available from: http://www.qclabequipment.com/VISCOSITY.html.
11. *A Basic Introduction to Viscometers & Viscometry* Rheosys 2011; Available from: http://www.rheosys.com/intro.html.
12. Webster, J.G., *Mechanical Variables Measurement-Solid, Fluid, and Thermal*. 1999: CRC Press.
13. M. Fritz, E.H., *Density Measurement*, in *Mass and Weight Measurement*. 1999.
14. Paredes, X., et al., *Study of the effects of pressure on the viscosity and density of diisodecyl phthalate.* Journal of Chemical Thermodynamics, 2009. **41**(9): p. 1007-1015.
15. Lundstrum, R., et al., *Measurement of the Viscosity and Density of Two Reference Fluids, with Nominal Viscosities at T = 298 K and p = 0.1 MPa of (16 and 29) mPa·s, at Temperatures between (298 and 393) K and Pressures below 55 MPa.* Journal of Chemical & Engineering Data, 2005. **50**(4): p. 1377-1388.

16. Audonnet, F. and A.A.H. Padua, *Simultaneous measurement of density and viscosity of n-pentane from 298 to 383 K and up to 100 MPa using a vibrating-wire instrument.* Fluid Phase Equilibria, 2001. **181**(1-2): p. 147-161.
17. Padua, A.A.H., et al., *Density and viscosity measurements of 1,1,1,2-tetrafluoroethane (HFC-134a) from 199 K to 298 K and up to 100 MPa.* Journal of Chemical and Engineering Data, 1996. **41**(4): p. 731-735.
18. Seibt, D., et al., *Simultaneous Measurements on Helium and Nitrogen with a Newly Designed Viscometer-Densimeter over a Wide Range of Temperature and Pressure.* Journal of Chemical and Engineering Data, 2009. **54**(9): p. 2626-2637.
19. Krall, A.H. and J.V. Sengers, *Simultaneous measurement of viscosity and density with an oscillating-disk instrument: The effect of fixed plates.* International Journal of Thermophysics, 2003. **24**(2): p. 337-359.
20. Evers, C., H.W. Losch, and W. Wagner, *An absolute viscometer-densimeter and measurements of the viscosity of nitrogen, methane, helium, neon, argon, and krypton over a wide range of density and temperature.* International Journal of Thermophysics, 2002. **23**(6): p. 1411-1439.
21. Thundat, T., P.I. Oden, and R.J. Warmack, *Microcantilever sensors.* Microscale Thermophysical Engineering, 1997. **1**(3): p. 185-199.
22. Boisen, A., et al., *Cantilever-like micromechanical sensors.* Reports on Progress in Physics, 2011. **74**(3): p. 036101.
23. Goeders, K.M., J.S. Colton, and L.A. Bottomley, *Microcantilevers: Sensing chemical interactions via mechanical motion.* Chemical Reviews, 2008. **108**(2): p. 522-542.
24. Hübert, T., et al., *Hydrogen sensors – A review.* Sensors and Actuators B: Chemical, 2011. **157**(2): p. 329-352.
25. Sader, J.E., *Frequency response of cantilever beams immersed in viscous fluids with applications to the atomic force microscope.* Journal of Applied Physics, 1998. **84**(1): p. 64-76.
26. Maali, A., et al., *Hydrodynamics of oscillating atomic force microscopy cantilevers in viscous fluids.* Journal of Applied Physics, 2005. **97**(7): p. 074907-074912.
27. J.B.Morion, S.T.T., *Classical Dynamics of Particles and Systems,*. 2004.
28. T. Kibble, F.B., *Classical Mechanics*. 2004: Imperial College Press
29. Toda, M., et al., *Measurements of the phase transition and the average length of the density fluctuation under supercritical fluid using micromechanical resonators.* Applied Physics Letters, 2011. **99**(7).
30. Youssry, M., et al., *A straightforward determination of fluid viscosity and density using microcantilevers: From experimental data to analytical expressions.* Sensors and Actuators a-Physical, 2011. **172**(1): p. 40-46.

31. Boskovic, S., et al., *Rheological measurements using microcantilevers.* Journal of Rheology, 2002. **46**(4): p. 891.
32. McLoughlin, N., S.L. Lee, and G. Hähner, *Simultaneous determination of density and viscosity of liquids based on resonance curves of uncalibrated microcantilevers.* Applied Physics Letters, 2006. **89**(18): p. 184106.
33. Shih, W.Y., et al., *Simultaneous liquid viscosity and density determination with piezoelectric unimorph cantilevers.* Journal of Applied Physics, 2001. **89**(2): p. 1497.
34. Wilson, T.L., G.A. Campbell, and R. Mutharasan, *Viscosity and density values from excitation level response of piezoelectric-excited cantilever sensors.* Sensors and Actuators A: Physical, 2007. **138**(1): p. 44-51.
35. Agoston, A., F. Keplinger, and B. Jakoby, *Evaluation of a vibrating micromachined cantilever sensor for measuring the viscosity of complex organic liquids.* Sensors and Actuators A: Physical, 2005. **123-124**: p. 82-86.
36. Bircher, B.A., et al., *Real-time viscosity and mass density sensors requiring microliter sample volume based on nanomechanical resonators.* Anal Chem, 2013. **85**(18): p. 8676-83.
37. Loui, A., et al., *Detection and discrimination of pure gases and binary mixtures using a dual-modality microcantilever sensor.* Sensors and Actuators A: Physical, 2010. **159**(1): p. 58-63.
38. Xu, Y., et al., *Viscous damping of microresonators for gas composition analysis.* Applied Physics Letters, 2006. **88**(14): p. 143513.
39. Marett, D., *A four quadrant photo detector for measuring laser pointing stability.* 2012.
40. *National Institute of Standards and Technology, Thermophysical properties of carbon dioxide* 2011.
41. Seitz, J.C., J.G. Blencoe, and R.J. Bodnar, *Volumetric properties for {(1 −x)CO2+xCH4}, {(1 −x)CO2+xN2}, and {(1 −x)CH4+xN2} at the pressures (9.94, 19.94, 29.94, 39.94, 59.93, 79.93, and 99.93) MPa and temperatures (323.15, 373.15, 473.15, and 573.15) K.* The Journal of Chemical Thermodynamics, 1996. **28**(5): p. 521-538.
42. Esper, G.J., et al., *Volumetric behavior of near-equimolar mixtures for CO2+CH4 and CO2+N2.* Fluid Phase Equilibria, 1989. **49**(0): p. 35-47.
43. B.E.Poling, J.M.P., J.P. O Connell, *The properties of gases and liquids*. Vol. 5. 2001, New York: McGraw-Hill.
44. Kestin, J. and W. Leidenfrost, *The effect of pressure on the viscosity of N2CO2 mixtures.* Physica, 1959. **25**(1–6): p. 525-536.
45. Hanley, H.J.M., *Prediction of the viscosity and thermal conductivity coefficients of mixtures.* Cryogenics, 1976. **16**(11): p. 643-651.

A.1 Raw Experimental Data

A.1. Raw Data for Nitrogen and Argon Measurements

Table A.1: Raw data for Argon at 308.15 K with 200 μm cantilevers

P(MPa)	fR (Hz)	f0 (Hz)	Q-factor
24.59	15827.96	15858.80	11.35
23.63	15945.94	15977.18	11.33
22.60	16035.21	16063.26	12.02
21.56	16294.08	16321.25	12.34
20.51	16403.60	16427.74	13.11
19.48	16563.38	16589.85	12.53
18.48	16711.56	16733.76	13.75
17.49	16862.45	16887.29	13.07
16.40	17092.30	17116.24	13.23
15.44	17228.27	17248.49	14.62
14.36	17438.29	17460.41	14.10
13.24	17554.98	17574.45	15.03
12.31	17720.32	17739.16	15.39
11.08	17954.98	17974.21	15.30
10.11	18146.59	18163.56	16.38
9.06	18367.48	18381.42	18.16
8.07	18551.04	18565.45	17.96
7.00	18819.83	18833.14	18.82
5.94	19065.32	19078.00	19.41
4.97	19333.80	19343.97	21.81
3.86	19590.28	19599.21	23.51
2.86	19877.05	19883.35	28.11
1.82	20170.75	20175.11	34.12
1.02	20437.43	20440.27	42.46
0.47	20620.63	20622.40	54.08
0.35	20665.00	20666.42	60.31

Table A.2: Raw data for Nitrogen at 308.15 K with 200 µm cantilevers

P(MPa)	f_R (Hz)	f_0 (Hz)	Q-factor
22.76	17440.51	17459.35	15.23
21.53	17540.02	17557.21	15.98
19.63	17708.52	17724.26	16.78
18.87	17837.57	17853.31	16.85
17.92	17927.49	17943.25	16.88
17.07	18052.32	18066.87	17.66
16.20	18141.98	18156.08	17.95
15.24	18252.48	18265.77	18.54
14.38	18355.69	18368.92	18.64
13.57	18460.71	18472.67	19.66
12.67	18567.64	18580.06	19.40
11.85	18689.36	18700.84	20.21
11.02	18820.26	18830.76	21.36
10.11	18948.70	18959.94	20.60
9.30	19053.79	19063.19	22.53
8.42	19200.74	19208.84	24.47
7.45	19338.43	19345.40	26.36
6.58	19478.57	19485.86	25.86
5.73	19641.03	19647.47	27.70
4.91	19763.03	19768.87	29.15
4.21	19886.73	19892.04	30.66
3.55	20014.60	20019.15	33.19
2.68	20175.91	20179.63	36.87
1.99	20334.17	20336.68	45.08
1.12	20516.60	20518.35	54.24
0.48	20678.94	20679.97	70.79

A.2. Raw Data for CO_2 - N_2 Binary Mixture Measurements

Table A.3: Raw data for CO_2 at 308.15 K with 200 µm cantilevers

P(MPa)	f_R (Hz)	f_0 (Hz)	Q-factor
22.76	12444.25	12508.11	7.01
22.12	12440.02	12504.08	7.00
21.45	12484.00	12548.15	7.00
20.04	12487.70	12551.19	7.05
19.35	12517.17	12582.28	6.97
18.71	12565.88	12629.46	7.06
17.93	12636.46	12700.03	7.08
17.17	12724.85	12782.98	7.43
14.34	12738.89	12797.49	7.40
15.90	12769.74	12828.18	7.42
15.20	12821.04	12876.57	7.62
14.51	12889.94	12946.35	7.58
13.91	12893.03	12949.99	7.55
13.12	12971.32	13024.48	7.83
12.48	13039.26	13093.46	7.78
11.77	13185.02	13236.27	8.04
11.02	13238.36	13287.67	8.22
10.38	13441.83	13492.73	8.18
9.70	13516.67	13562.67	8.59
9.03	13797.35	13837.90	9.25
8.70	13915.14	13958.58	8.98
8.31	14308.02	14341.67	10.34
8.18	14665.82	14699.09	10.52
8.03	15689.78	15720.48	11.32
7.92	16089.77	16114.96	12.66
7.64	16694.77	16715.59	14.17
6.87	17567.03	17584.28	16.00

6.16	18137.1	18175.9	17.24
5.46	18531.3	18542.8	20.13
4.82	18859.7	18869.6	21.83
4.14	19152.1	19160.5	23.95
3.46	19452.4	19459.1	26.95
2.77	19754	19759.5	29.94
2.1	19992.4	19996.8	33.71
1.39	20271.7	20274.6	41.81
0.68	20550.2	20551.8	57.05
0.34	20699.3	20700.2	75.12

Table A.4: Raw data for 0.8 CO_2 - 0.2 N_2 at 308.15 K with 200 µm cantilevers

P(MPa)	f_R (Hz)	f_0 (Hz)	Q-factor
22.76	13610.09	13654.62	8.77
21.97	13706.80	13750.47	8.88
21.36	13723.21	13765.23	9.06
20.67	13799.22	13839.60	9.27
20.02	13881.10	13923.40	9.08
19.32	13942.43	13983.91	9.19
18.63	14039.55	14079.53	9.39
17.88	14161.03	14200.26	9.52
17.26	14267.71	14303.26	10.04
16.55	14487.29	14519.46	10.63
15.86	14639.53	14673.28	10.44
15.17	14785.33	14816.27	10.97
14.42	15009.51	15038.76	11.35
13.81	15169.85	15198.47	11.53
13.11	15298.68	15322.33	12.73
12.43	15624.78	15651.37	12.14
11.73	15904.27	15926.75	13.31
11.05	16171.50	16198.38	12.28
10.36	16571.47	16598.59	12.44
9.67	16743.83	16765.12	14.12
8.96	16958.97	16976.39	15.62

8.69	17161.6	17176.3	17.13
8.27	17359.3	17372.5	18.14
8.12	17334.1	17347.1	18.24
8.01	17477	17489.7	18.57
7.9	17562.9	17575.4	18.72
7.68	17657.3	17669.4	19.12
7.58	17744.4	17757.4	18.54
6.89	18027.2	18038.3	20.15
6.21	18193.8	18204.1	21.03
5.53	18600.9	18610	22.63
4.82	18879.1	18887.2	24.22
4.13	19144.4	19150.8	27.42
3.4	19362.6	19368.3	29
2.76	19596.2	19601.2	31.34
2.04	19837.1	19841.1	35.1
1.38	20071.9	20074.7	42.56
0.7	20321.7	20323.2	58.19
0.35	20445.8	20446.9	69.16

Table A.5: Raw data for 0.6 CO_2 - 0.4 N_2 at 308.15 K with 200 µm cantilevers

P(MPa)	f_R (Hz)	f_0 (Hz)	Q-factor
22.51	15086.76	15118.40	10.95
22.04	15159.02	15190.42	11.00
21.31	15258.70	15290.66	10.95
20.75	15322.74	15354.05	11.12
20.05	15442.04	15466.23	12.77
19.30	15570.22	15597.67	12.00
18.64	15689.25	15715.39	12.28
17.95	15819.24	15845.01	12.45
17.28	15919.81	15943.77	12.91
16.55	16077.01	16099.60	13.36
15.88	16202.15	16224.35	13.54
15.18	16353.12	16373.03	14.35
14.49	16569.44	16590.97	13.94
13.73	16715.19	16734.22	14.83

13.11	16864.2	16883.1	14.97
12.42	17059.7	17077.8	15.4
11.72	17235.4	17255.5	14.79
11.05	17438.9	17454.4	16.81
10.34	17608.2	17623.7	16.91
9.65	17814.7	17827.2	18.91
8.95	18035.7	18049.9	17.83
8.27	18219.9	18233.2	18.55
7.91	18325.8	18337.9	19.48
7.58	18408.6	18419.2	20.88
6.91	18648.5	18659	21.02
6.17	18819.8	18828.6	23.27
5.52	19001.8	19010.6	23.26
4.85	19210.6	19217.8	25.9
4.13	19435.4	19441.9	27.41
3.45	19630.9	19636.6	29.37
2.76	19830.5	19835.5	31.5
2.05	20039.4	20043	37.3
1.39	20241.7	20244.5	42.36
0.7	20452.3	20453.8	59.21
0.34	20568	20569	73.95

Table A.6: Raw data for 0.4 CO_2 - 0.6 N_2 at 308.15 K with 200 µm cantilevers

P(MPa)	f_R (Hz)	f_0 (Hz)	Q-factor
22.75	16124.20	16149.26	12.72
22.11	16175.22	16199.91	12.86
21.40	16280.66	16305.10	12.93
20.73	16397.22	16421.44	13.12
20.02	16495.05	16517.79	13.49
19.25	16579.06	16602.66	13.27
18.66	16701.28	16726.20	12.97
17.91	16808.64	16830.87	13.78
17.21	16940.25	16961.10	14.31
16.56	17039.42	17058.69	14.90

15.83	17155	17231.7	14.52
15.15	17233.5	17253.7	14.65
14.5	17366.7	17385.6	15.19
13.8	17533.6	17550.1	16.35
13.08	17674.4	17691.6	16.09
12.42	17794.2	17812.4	15.66
11.73	17930	17945.8	16.88
11.02	18059.2	18072.9	18.19
10.34	18224.5	18239.4	17.55
9.63	18357	18369.9	18.99
8.95	18506.8	18519.5	19.17
8.2	18649.8	18659.8	21.67
7.87	18750.7	18763.3	19.34
7.57	18817.4	18827.7	21.36
6.88	18995.8	19005.6	22.09
6.2	19106.5	19116.1	22.35
5.51	19304	19311.8	24.97
4.8	19485.1	19492.1	26.37
4.12	19669.2	19675.9	27.28
3.41	19835.3	19840.3	31.59
2.75	20014.7	20018.9	34.67
2.05	20204.7	20208	38.99
1.36	20397.1	20399.5	45.62
0.68	20596.9	20598.2	61.69
0.33	20713.8	20714.7	78.55

Table A.7: Raw data for 0.2 CO_2 - 0.8 N_2 at 308.15 K with 200 µm cantilevers

P(MPa)	f_R (Hz)	f_0 (Hz)	Q-factor
22.80	16782.80	16803.70	14.22
22.07	16900.90	16925.66	13.12
21.37	16955.01	16977.09	13.91
20.69	17004.14	17027.04	13.65
20.02	17105.92	17124.77	15.11
19.34	17143.67	17163.67	14.66
18.66	17245.92	17265.03	15.16
17.92	17429.20	17446.74	15.98
17.26	17475.27	17494.28	15.22
16.57	17566.68	17584.62	15.73
15.84	17695.40	17715.91	14.75
15.15	17770.38	17784.31	17.96
14.45	17869.50	17884.59	17.32
13.81	17979.78	17994.18	17.72
13.07	18068.31	18083.98	17.13
12.39	18201.83	18212.62	20.65
11.72	18318.51	18331.76	18.98
11.00	18458.83	18473.83	17.59
10.31	18577.22	18589.37	19.58
9.66	18718.73	18730.42	20.70
8.94	18807.59	18819.40	20.25
8.25	18929.89	18940.76	20.99
7.57	19070.40	19080.05	22.24
6.87	19218.52	19227.76	22.94
6.17	19342.30	19350.59	24.17
5.49	19481.59	19489.20	25.33
4.78	19642.92	19649.52	27.48
4.12	19782.90	19789.06	28.42
3.42	19953.73	19959.36	29.78
2.74	20118.22	20121.94	36.77
2.03	20270.56	20273.83	39.58
1.36	20441.82	20444.38	44.99
0.68	20635.17	20636.50	62.49
0.37	20734.02	20734.98	73.63

Table A.8: Raw data for N_2 at 308.15 K with 200 µm cantilevers

P(MPa)	f_R (Hz)	f_0 (Hz)	Q-factor
22.74	17325.39	17344.17	15.20
22.07	17400.25	17418.56	15.43
21.39	17464.51	17482.27	15.69
20.70	17520.72	17538.63	15.65
19.97	17605.43	17622.74	15.97
19.31	17680.77	17698.24	15.93
18.61	17693.40	17709.60	16.54
17.92	17766.20	17782.20	16.67
17.23	17849.73	17865.16	17.01
16.55	17931.53	17946.23	17.48
15.86	18008.00	18022.66	17.54
15.14	18137.00	18151.78	17.54
14.49	18223.12	18237.33	17.92
13.80	18306.00	18320.05	18.06
13.08	18401.08	18409.92	18.73
12.38	18497.49	18510.38	18.96
11.73	18604.44	18616.48	19.66
11.03	18686.55	18697.96	20.25
10.32	18786.43	18797.26	20.83
9.65	18891.57	18901.91	21.39
8.96	18992.46	19002.25	22.02
8.28	19098.98	19108.43	22.50
7.59	19208.15	19216.63	23.81
6.89	19322.57	19327.63	24.96
6.22	19436.34	19443.94	25.31
5.49	19565.15	19571.87	27.00
4.82	19689.52	19695.58	28.51
4.13	19816.63	19821.68	31.33
3.42	19951.62	19956.16	33.16
2.74	20081.80	20085.96	34.80
2.05	20209.60	20212.74	40.12
1.35	20370.32	20372.44	49.08
0.67	20530.93	20532.25	62.46
0.32	20626.91	20627.69	81.30

A.3. Raw Data for CO_2 Measurements at 304.45 K

Table A.9: Raw data for CO_2 at 304.45 K with 200 µm cantilevers

P(MPa)	f_R (Hz)	f_0 (Hz)	Q-factor
24.19	11930.22	12002.88	6.44
21.66	12014.12	12087.82	6.43
19.03	12137.36	12217.81	6.78
15.62	12314.04	12375.60	7.10
12.91	12480.48	12536.54	7.49
11.00	12712.67	12767.00	7.67
9.89	12916.19	12967.05	7.99
9.25	13093.84	13145.61	7.98
8.56	13305.63	13352.38	8.46
8.14	13426.11	13471.65	8.61
7.85	14690.24	14734.73	9.11
7.70	15345.39	15384.45	9.93
7.47	16571.86	16592.37	14.26
7.29	16831.32	16849.36	15.29
7.10	17030.59	17046.71	16.27
6.58	17202.93	17218.91	16.86
6.34	17677.26	17681.52	18.70
4.31	18701.62	18709.60	24.22
3.50	19026.02	19032.54	27.02

Table A.10: Raw data for CO_2 at 304.45 K with 300 µm cantilevers

P(MPa)	f_R (Hz)	f_0 (Hz)	Q-factor
24.14	5610.08	5683.75	4.41
21.68	5657.30	5729.92	4.46
19.04	5721.34	5791.51	4.56
15.71	5806.99	5872.86	4.73
12.93	5904.08	5967.02	4.88
10.99	5998.18	6055.85	5.14
9.93	6094.12	6146.27	5.44
9.27	6153.71	6208.84	5.33
8.52	6288.51	6337.19	5.73
8.11	6381.37	6428.77	5.86
7.87	6550.47	6597.10	5.98
7.71	6709.79	6752.17	6.33
7.46	7775.00	7797.20	9.38
7.28	7964.33	7983.06	10.33
7.10	8079.47	8096.72	10.85
6.87	8166.67	8183.05	11.18
6.34	8391.18	8404.20	12.71
5.52	8629.76	8640.52	14.18
4.30	8898.30	8906.79	16.20
3.49	9061.70	9068.67	18.07

Table A.11 Raw data for CO_2 at 304.45 K with 400 µm cantilevers

P(MPa)	f_R (Hz)	f_0 (Hz)	Q-factor
24.15229	3000.593	3059.227	3.629233
21.67708	3028.774	3085.277	3.711967
19.04329	3062.619	3117.134	3.797667
15.66486	3111.349	3161.57	3.986833
12.92765	3170.258	3217.058	4.161503
10.99712	3229.236	3275.609	4.218033
9.942222	3279.313	3322.025	4.423967
9.266537	3319.144	3360.684	4.515333
8.521905	3365.779	3405.877	4.624633
8.10822	3411.608	3450.758	4.710333
7.866904	3484.34	3519.379	5.0268
7.706026	3527.917	3563.38	5.025733
7.467009	4226.266	4245.225	7.4904
7.278552	4289.861	4306.806	7.979933
7.087798	4370.985	4386.421	8.436533
6.867166	4447.557	4461.451	8.967167
6.339718	4565.015	4577.813	9.4645
5.513498	4702.791	4713.817	10.34487
4.302321	4867.998	4876.304	12.1217
3.479548	4964.355	4971.551	13.14663

VITA

Gamze Eriş was born in Bursa, Turkey, on May 9, 1990. She received her B.Sc. Degree in Chemical and Biological Engineering from Koç University, Istanbul, in 2013. From September 2013 to July 2015 she worked as teaching and research assistant at Koç University, Istanbul, Turkey. She has worked on "Determination of Density and Viscosity of Fluids and Fluid Mixtures using Frequency Response of Microcantilevers" during her M.S. study.